Eco-friendly synthesis of Ag-NPs using Endostemon viscosus (Lamiaceae) antibacterial, antioxidant, larvicidal, photocatalytic dye degradation activity and toxicity in zebrafish embryos

Chinnasamy, R.; Chinnaperumal, K.; Venkatesan, M.; Jogikalmat, K.; Cherian, T.; Peijnenburg, W.J.G.M.; Malafaia, G.

Environmental Research 218 (2023) 114946

Contents lists available at ScienceDirect

Environmental Research

journal homepage: www.elsevier.com/locate/envres

Eco-friendly synthesis of Ag-NPs using *Endostemon viscosus* (Lamiaceae): Antibacterial, antioxidant, larvicidal, photocatalytic dye degradation activity and toxicity in zebrafish embryos

Ragavendran Chinnasamy [a], Kamaraj Chinnaperumal [b], Manigandan Venkatesan [c], Krithikadatta Jogikalmat [a], Tijo Cherian [d], Peijnenburg Willie [e,f], Guilherme Malafaia [g,h,i,j,*]

[a] Department of Conservative Dentistry and Endodontics, Saveetha Dental College and Hospitals, Saveetha Institute of Medical and Technical Sciences (SIMATS), Chennai, 600 077, India
[b] Interdisciplinary Institute of Indian System of Medicine (IIISM), Directorate of Research and Virtual Education, SRM Institute of Science and Technology (SRMIST), Kattankulathur, Chennai, 603203, Tamil Nadu, India
[c] Department of Medicine, University of Texas Health Science Center, San Antonio, TX, USA
[d] Department of Ocean Studies and Marine Biology, Pondicherry University, Port Blair Campus, Brookshabad, Port Blair, Andamans, 744112, India
[e] Leiden University, Institute of Environmental Sciences (CML), P.O. Box 9518, 2300 RA, Leiden, the Netherlands
[f] National Institute of Public Health and the Environment (RIVM), Center for Safety of Substances and Products, P.O. Box 1, Bilthoven, the Netherlands
[g] Laboratory of Toxicology Applied to the Environment, Goiano Federal Institute, Urutaí, GO, Brazil
[h] Post-Graduation Program in Conservation of Cerrado Natural Resources, Goiano Federal Institute, Urutaí, GO, Brazil
[i] Post-Graduation Program in Ecology, Conservation, and Biodiversity, Federal University of Uberlândia, Uberlândia, MG, Brazil
[j] Post-Graduation Program in Biotechnology and Biodiversity, Federal University of Goiás, Goiânia, GO, Brazil

ARTICLE INFO

Keywords:
Green nanoparticles
Bionanotechnology
Ecotoxicology
Medicinal potential
Biosynthesis of nanomaterials

ABSTRACT

Nanotechnology is a multidisciplinary area of study that has grown significantly in serving many functions and impacting human society. New fields of science have been facilitated by the clean, non-toxic, and biocompatible nature of plant-derived nanoparticles. The present study deals with the first green synthesis of silver nanoparticles (Ag-NPs) using *Endostemon viscosus,* and their synthesized Ag NPs were characterized by different spectral methods (UV–vis Spectroscopy, Fourier Transform Infrared Spectroscopy (FTIR), X-ray diffraction Spectroscopy (XRD), Transmission Electron Microscopy (TEM) and Energy dispersive X-ray Spectroscopy (EDAX). The change initially observed the production of Ag-NPs in color from green to ash and then confirmed by SPR band at 435 nm in UV–vis spectral analysis. The FTIR findings indicate that many functional groups belong to the pharmaceutically useful phytochemicals, which interact as reducing, capping, and stabilizing agents in synthesizing silver nanoparticles. The predominant peaks in the XRD pattern belong to the planes 210°, 111°, 200°, 241°, and 311° and thus demonstrated the Ag-NPs FCC crystal structure. TEM analysis exhibited spherical-shaped particles with an average size of 13 nm, and the EDAX band showed a distinctive metallic silver peak at 3.0 keV. The antibacterial activity of Ag-NPs tested to show a maximum zone of inhibition of 19 mm for *Staphylococcus aureus* and 15 mm for *Escherichia coli* at 100 μg/mL, respectively. Bio-fabricated Ag-NPs were assessed for antioxidant activity (DPPH with % inhibition 57.54% and FRAP with % inhibition 70.89%). The biosynthesized Ag-NPs demonstrated potential larvicidal efficacy against *Aedes aegypti* with more than 90% at 250 μg/mL. Histological profiles were altered while treating with Ag-NPs at 250 μg/mL. The photocatalytic activity of synthesized *E. viscosus* Ag-NPs was tested against methylene blue (MB) and crystal violet (CV), and the maximum degradation efficiency was found as 90 and 94%, respectively. Furthermore, the toxicity test on zebrafish embryos demonstrated that aberrations have only been induced at concentrations higher than 500 μg/mL. We conclude that the greenly produced Ag-NPs may find use in biomedical applications based on bacteria and cost-effective industrial wastewater treatment.

* Corresponding author. Laboratory of Toxicology Applied to the Environment, Goiano Federal Institution, Urutaí Campus, Rodovia Geraldo Silva Nascimento, 2,5 km, Zona Rural, Urutaí, GO, CEP: 75790-000, Brazil.
E-mail address: guilhermeifgoiano@gmail.com (G. Malafaia).

https://doi.org/10.1016/j.envres.2022.114946
Received 7 September 2022; Received in revised form 18 November 2022; Accepted 23 November 2022
Available online 6 December 2022

1. Introduction

Antibiotic resistance is an important global issue that has driven research toward developing novel biomolecules with widespread antimicrobial activities (Aribisala and Sabiu, 2022; Bostanci et al., 2022). Recently, there has been an increase in the prevalence of antibiotic-resistant bacteria that cause nosocomial infections (Frieri et al., 2017). Additionally, the increase in new outbreaks carried on by bacterial mutations necessitates the development of novel biologically active ingredients (Tiri et al., 2022). On the other hand, dyes are used in many industries, such as those that work with textiles, paper, leather, food, and cosmetics (Gupta et al., 2022). The most used dye for dying cotton, wool, and silk is methylene blue (MB) and crystal violet (CV). Finding secure and efficient methods to minimize environmental degradation is the main component of its toxicity and persistence in the environment (Subramaniam et al., 2022). Several earlier studies have examined the photocatalytic decomposition of environmental contaminants using nanoparticles synthesized by plants. Negi et al. (2022) reported a green approach for synthesizing silver nanoparticles by *Smilax aspera* and its applications in photocatalytic dye degradation. Additionally, various plants have been exploited for their ability to biosynthesize several nanoparticles, including silver and zinc nanoparticles, and their application in the process of photocatalytic dye degradation (Rajasekar et al., 2022; Tiri et al., 2022; Lin et al., 2022; Karimi et al., 2022b). Mosquitoes are among the most prevalent vector species and can spread diseases like Ross River fever, West Nile virus, Richard virus, dengue fever, zika virus, malaria, and dengue fever (Foster and Walker, 2019). Every year, this leads to infections like skin damage, sore muscles and joints, conjunctivitis, and hemorrhagic fever, which cause illness, mental illness, and death (Musiime et al., 2022). Mainly found in tropical and subtropical areas are *Aedes aegypti*, *Aedes albopictus*, and *Aedes vitattus* (Wilson-Bahun et al., 2020). Due to a lack of information and suitable insecticides, vector management is a severe problem in developing countries like India. DDT, other organochlorine insecticides, organophosphates, and synthetic pyrethroids were used against *Ae. aegypti* during the twentieth century in various countries around the world. Continuous synthetic chemical insecticides develop mosquito resistance and reduce natural resources and safe, cheap alternatives to insecticides (Khursheed et al., 2022). Therefore, developing new and better mosquito control is urgently needed to increase human life (Şengül Demirak and Canpolat, 2022).

Nanotechnology can be used to address these urgent environmental problems because it offers excellent activity and high efficiency in a variety of applications across many fields, including chemistry, electronics, medicine, materials, and biology (Gulbagca et al., 2019; Karimi et al., 2022a; Karimi et al., 2022b; K. H. Liang et al., 2022). For this, several production routes of NPs have been described in the literature, including wet chemical processing (Nikam et al., 2018; Yousaf et al., 2020), micro-emulsion techniques (Bibi et al., 2021; Y. Liang et al., 2022), thermal reduction (Salem et al., 2017), as well as biosynthesis from microorganisms and/or extracts of plants have (Mustapha et al., 2022; Jeevanandam et al., 2022; Patel, 2022). However, several other studies have also shown that, among so disponible methods, a plant-mediated biosynthesis of metal NPs is highly advantageous (Ahmad et al., 2020; Jadoun et al., 2021). Recent research on green synthesis uses a wide range of organisms, such as bacteria, plants, algae, and fungi metabolites, acting as reducing agents (Jeong et al., 2022). Using biomolecules as surfactants in the surface coating during the production of nanoparticles results in high stability and biocompatibility qualities (Abadi et al., 2022). Due to their functional surfaces, and hydrophilic properties, bio-capped nanoparticles are significantly important (Dheyab et al., 2020; Seckin et al., 2022). According to Yang et al. (2020), the *Crocus sativus* L. extract used in the green synthesis of Ag–Pt bimetallic possesses excellent photocatalytic activity against MB as well as antibacterial and antifungal properties. Recently, Karimi et al. (2022) investigated the antibacterial efficacy of Ag-based palladium nanoparticles that exhibited strong growth inhibitory activities against Gram-positive and Gram-negative bacteria. A suitable replacement for larvicides made of plant-derived bioactive metabolites is silver nanoparticles (Ag-NPs), which are manufactured from extracts of different plants (Athanassiou et al., 2018). Additionally, Koduru Mallikarjuna and his team prove that the environmentally friendly synthesis of Pd–Ag/rGO nanoparticles using an extract of *Stevia* leaves creates hydrogen and antimicrobial activity (Mallikarjuna et al., 2021).

In addition, green synthesis boosts the potential of nanotechnology because it is an environmentally friendly, simple, stable, quick, and less expensive technique (Mughal and Hassan, 2022). Nanoparticles are typically made with aqueous metal solutions with an eco-friendly reducing agent, like a plant extract (Aygün et al., 2022). Metal ions can be changed to metal nanoparticles by plant metabolites with antioxidant or reducing abilities (Labulo et al., 2022). Flavonoids, proteins, polyphenols, amino acids, alkaloids, enzymes, reducing sugars, and various other bioactive substances are found in plant extracts and might play a role in the bio-reduction of metal ions to metal nanoparticles as well as in stabilizing/capping the metallic nanoparticles (Gebre, 2022; Ojha, 2022). Green synthesis of Ag-NPs with *Diospyros malabarica* fruit extract was used, and their cytotoxic, antibacterial, and catalytic properties were studied (Bharadwaj et al., 2021). The research also discusses the bactericidal, anticancer, and catalytic capabilities of green synthesized Ag and Pd-NPs (Aygün et al., 2020). In addition, Rajkumar and Sundar (2022) conducted the green synthesis of Ag-NPs from *Persea americana* showed potential antibacterial, antifungal, and antioxidant activities.

The biosynthesis of metallic nanoparticles opened the route for environmental protection and improvement by reducing harmful chemicals, minimizing biological hazards in biomedical applications, and using it for disinfection and the degradation of harmful pollutants. The novelty of this study is the use of *Endostemon viscosus* leaf extract as a potent reducing and capping agent for the first synthesis of Ag-NPs. The size and shape of nanoparticles were analyzed and structurally characterized using various spectroscopic and microscopic methods. The biological activities of bio-synthesized Ag-NPs have been studied, emphasizing their potential for photocatalytic activity methylene blue (MB) and crystal violet (CV), antibacterial, radical scavenging properties (DPPH and Reducing power assay), and larvicidal activity against *Aedes aegypti* and evaluate the toxicity profile of Ag-NPs in the zebrafish model.

2. Material and methods

2.1. Preparation of plant materials

The healthy and disease-free leaves of *Endostemon viscosus* were collected from Harur (Latitude: 12.046967, Longitude: 78.483273), Dharmapuri, Tamil Nadu, India. Like, 25 g of leaves were weighed and thoroughly washed three times with distilled water and with Millipore water to clean the leaves of debris and other impurities. The leaves were sliced into a fine powder before being mixed with 100 mL of Millipore water in a labeled conical flask and heated for 15 min. For further study, the plant extract was filtered using Whatman no. 1 filter paper and held at 4 °C.

2.2. Synthesis of Ag-NPs from leaf extract

To produce Ag-NPs, Milli Q water was used to make a 1 mM silver nitrate ($AgNO_3$) aqueous solution. 90 mL of a 1 mM $AgNO_3$ solution were treated with 10 mL of an aqueous extract within 4 h. The influence of temperature on the production of nanoparticles was investigated at 60 °C. The green-to-ash color change of the solution indicates the production of Ag-NPs from aqueous Ag ions and plant extract.

2.3. Characterization of green synthesized silver nanoparticles

2.3.1. UV–visible spectral analysis

The surface plasmon resonance (SPR) peak of synthesized AgNPs generated from *E. viscosus* extract was examined using a double–beam spectrophotometer (Shimadzu UV spectrophotometer, model UV-1800) with 1-nm specificity and a measuring range of 200–700 nm. Using distilled water, 10x dilutions of colloidal solutions resulting from the fabrication process were made (Nasir et al., 2022). Aliquots (1 mL) of the mixture were frequently taken to update the status of the bio-reduction of the Ag ion aqueous phase.

2.3.2. X-ray diffraction (XRD) pattern

To obtain a powder of nanomaterials, produced Ag-NPs in solutions were centrifuged at 10,000 rpm for 15 min at 4 °C. Then, 1 g of Ag-NP was placed into the sample container of the device for XRD examination, which was then used to analyze the particle's structure and shape using CuK radiation at a 40 kV voltage and 30 mA∘ power, like Amarasinghe et al. (2020). Diffracted intensities were used to calculate the Ag-NP's features. The scanning was performed with a Brucker X-ray diffractometer machine in Copper:Potassium (CuK) radiation with a time constant of 2 s.

2.3.3. Fourier transform infrared spectroscopy (FT-IR)

FTIR analysis of the Ag-NPs was carried out through potassium bromide (KBr) pellet procedure in FT-IR analysis (1:100 ratio), and the spectrum was recorded using Jasco FT/IR-6300 FTIR equipped with JASCO IRT-7000 Intron Infrared microscope (JASCO, Tokyo, Japan) using transmittance mode operating at a resolution of 4 cm-1. The powdered nanomaterials were examined in the mid-IR range of 400–4000 cm-1, according to Parthiban et al. (2019).

2.3.4. Energy dispersive X-ray spectroscopy (TEM) analysis

A transmission electron microscope has been used to examine the images of the Ag-NPs (TEM; JEOL, Model JFC-1600). The TEM measurements were conducted using a Hitachi H-7100 device with a 120 kV acceleration voltage and water as the solvent. Drops of the AgNPs solution were used to prepare the samples for TEM observation on a carbon-coated grid. After removing excess solution using blotting paper, the Ag-NPs solution on the TEM grid was allowed to air dry for a few hours. The EDX analysis was carried out through Hitachi model H-7100.

2.3.5. Photocatalytic activity

The photocatalytic activity of synthesized was studied using methylene blue (MB) crystal violet dyes (CV) as a model dye under natural sunlight irradiation, like Venkatesh et al. (2021), with minor modifications. For this, 50 mg of biosynthesized Ag-NPs were added to 50 mL of aqueous dye solutions (at 20 mg/L), and the mixture was exposed to sunlight for 180 min. At appropriate intervals of 30 min, 2 mL of the reaction solution were collected, and the solution's absorption intensity was recorded using a UV–visible spectrophotometer at 663 nm. The solution's color vanished, indicating that the catalyst was working well. The photocatalytic experiment was conducted between 10:30 a.m. and 2:30 p.m. under a cloudless, clear sky. The photocatalytic study's average solar light intensity was approximately 0.95 × 105 lx.

2.4. Microbial assay

2.4.1. Preparation of bacterial inoculums

A 24-h Muller-Hinton broth (MHB, HI-Media, Mumbai) culture of tested bacteria (*Staphylococcus aureus* ATCC-25923 and *Escherichia coli* ATCC-25922) was grown in an orbital shaking incubator without agitation for 24 h at 37 °C. Fresh Mueller-Hinton broth has been used to reduce the culture to obtain an optical density equivalent to 0.5 (i.e., 10^5–10^6 CFU/mL using MacFarland's standard).

2.4.2. Agar well diffusion method

All strains of microorganisms were kept in glycerol stocks and received from the Department of Microbiology at Mohan Kumaramangalam Medical College in Salem, Tamil Nadu, India, for further examination (CLSI, 2015; Murugan et al., 2020). The antibacterial activity of the biosynthesized Ag-NPs was investigated using the agar well diffusion method against clinical pathogenic organisms, which is widely used to evaluate *in vitro* evaluating antimicrobial activity (Valgas et al., 2007; Balouiri et al., 2016). The pure cultures of the organism were sub-cultured on Muller-Hinton broth at 37 °C on a rotary shaker at 200 rpm. Muller-Hinton agar powder (3.8 g) was melted in 100 mL of water by gradually heating it in a beaker. The agar solution was sterilized by autoclaving at 15 lbs pressure at 121 °C for 15 min. The sample was chilled to 40–45 °C in a laminar hood. After that, the liquid was added to Petri-dishes with relatively identical agar thickness (2.5 mm). The dishes were left to cool for much time (25–35 min) for the agar medium to solidify. The Muller-Hinton agar plates were prepared using gel puncture, and each strain was evenly swabbed on the separate plates using sterile cotton swabs. Ag-NPs solutions at 50 and 100 μg/mL (obtained from a stock solution at 1 mg/mL) were placed in the wells on all the plates using a micropipette. The covered dishes were rapped well by paraffin film to seal them. Dimethyl sulfoxide (at 10%) was used as a negative control, and the antibiotics chloramphenicol (at 50 and 100 μg/mL) were used as a positive control. The overall handling was carried out within the laminar hood in front of a spirit light. The zone of inhibition was assessed following a 24 h incubation period at 37 °C.

2.5. In vitro antioxidant assays

2.5.1. DPPH free radical scavenging assay

To assess the antioxidant potential of Ag-NPs, we used the 1,1-diphenyl-2-picrylhydrazyl (DPPH) radical scavenging method, according to Akgul et al. (2022), with some modifications. Briefly, different amounts of aqueous leaf extract of *E. viscosus* and biosynthesized AgNPs (50–250 μg/mL) were combined with 1 μL of DPPH (at 0.1 mM in ethanol). After shaking, the reaction suspension was left to sit in the dark for 30 min. Against a white reference, the absorbance at 517 nm was measured (ethanol). The reference was (ascorbic acid). The reaction mixture's lower absorbance suggested a maximum level of scavenging ability. Equation (1) was used to calculate the proportion of free radicals that were inhibited or scavenged, according to Xiao et al. (2020):

$$\text{Inhibition ratio } (\%) = \frac{(A1 - A2)\ x\ 100}{A1} \quad (1)$$

where "A1" is the absorbance of the addition of ethanol instead of the testing sample and "A2" is the absorbance of the testing sample solution.

2.5.2. Reducing power assay

The reducing power evaluation was done using Erenler & Dag et al. (2022) method, with minor modifications. Briefly, 500 μL of aqueous leaf extract of *E. viscosus* and biosynthesized AgNPs (at different concentrations; 50–250 μg/mL) were combined with phosphate buffer (to 0.2 M, pH 6.6) and potassium ferricyanide (at 1%) and, subsequently, the reaction mixture was incubated for 20 min at 50 °C. Then, this mixture was added to 2.5 mL of trichloroacetic acid (at 10%), which was centrifuged at 3000 rpm for 10 min. To determine the absorbance at 700 nm, 2.5 mL of the supernatant mixture was combined with 2.5 mL of distilled water and 0.5 mL of $FeCl_3$ (to 0.01%). Ascorbic acid served as the standard, with phosphate buffer functioning as the control. According to Oyaizu (19886), the reaction solution's increased absorbance indicated enhanced reducing power.

2.6. Larvicidal activity

2.6.1. Collection of mosquitoes

Laboratory culture of mosquito larvae *Ae. aegypti* was obtained from the National Centre for Disease Control (NCDC), Mettupalayam, Tamil Nadu, India. All the larvae were incubated in plastic containers supplied with tap water. All studies were performed under 14:10 light/dark photoperiod cycles at 27 ± 2 °C and humidity at 75–85%. Dog biscuits and yeast granules were served to larvae in a 3:1 ratio. In the laboratory, the cultures were kept alive and developed.

2.6.2. Larvicidal bioassay

With some changes, a larvicidal bioassay was performed according to WHO (2005) protocols. In a 500 mL glass beaker with 249 mL of dechlorinated water and the desired amounts of fluid plant extract, *Ae. aegypti* larvae of the first to the fourth instar were added. Dechlorinated tap water was used for the control group. The number of dead larvae was recorded after 24 h of exposure, and the LC_{50} and LC_{90} values were calculated. The toxicity of the biosynthesized Ag-NPs was evaluated by applying a multi-concentration test, which included control and different concentrations of Ag-NPs (50, 100, 150, 200, and 250 μg/mL). Each test was performed by placing 25 mosquito larvae into 100 mL of distilled water with biosynthesized Ag-NPs into a glass beaker. Three replicates of each concentration were used in each test, along with a predetermined control group consisting of DMSO (at 10%) and distilled water. Mortality was evaluated to examine the acute effects on *Ae. aegypti* mosquito larvae after 24 h. The dead larvae in five replicates were combined and expressed as a percentage of larval mortality for each concentration. According to Abbott's formula, the correct mortality was determined (Abbott, 1925).

2.6.3. Histological analysis

A qualitative histological investigation of vulnerable larvae also was done. The deceased larvae were dehydrated in ethyl alcohol for 24 h, kept in 10% buffered formaldehyde, then cleaned with xylene. The prepared larvae were encased in slabs of molten paraffin. The embedded paraffin was sectioned into 5 mm thick sections and stained with hematoxylin and eosin using a rotary microtome. The sections were evaluated for abnormalities under a 400× magnification bright field light microscope and documented, like Ga'al et al. (2018) and Wilson et al. (2022).

2.7. Evaluation of silver nanoparticles toxicity in the non-target organism (ecotoxicity)

2.7.1. Fish embryo acute toxicity (FET) test

2.7.1.1. Fish and fish maintenance. For egg production, a breeding population of wild-type (ABWT) zebrafish (*Danio rerio*) aged (6–20 months) was used. The fishes were born and raised in a pumped back system (Aquaschwarz, Germany) with a regular water exchange rate of 10% at 27 °C (pH 7.4, the conductivity of 550 μS, under a 14 h:10 h light-dark cycle - stock density of 5 adult fish/L and a sex ratio of 1:1). Fish were given finely ground dry feed (CIBA Fish Food, India) twice daily and *Artemia nauplii* once daily (Ocean Nutrition, Belgium).

2.7.1.2. Egg collection and experimental design. Fish were placed in aquariums the night before the experiment, at 27 °C, to induce breeding behavior. Pipette boxes that were empty and coated in mesh (4 mm × 4 mm) were immersed in the tanks and measured 10 × 6 × 4 cm in length, width, and height, respectively. Eggs were removed from the boxes the following day, around 2 h after the start of fish spawning, and washed in sterile water from the fish facility. Under the dissecting microscope (magnification ×6.3–40), fertile and unfertilized eggs could be differentiated from one another (Leica S6E, Germany). Fertilized eggs between stages of 4 and 128 cells were utilized for the fish embryo acute toxicity (FET) test.

FET test was conducted in accordance with OECD test guideline 236 at a temperature of 27 °C (OECD, 2012). Fertilized eggs were dispersed into 24 well plates with 2.5 mL of test solution each (Ref. 83.3922500, Sarstedt, Germany). From a standard solution mixed in sterile, facility-system-filtered water, six concentrations of biosynthesized Ag-NPs (0.25, 0.5, 50, 250, 500 μg/mL, and 1 mg/L) were developed (rearing medium). Each plate included 20 eggs suspended in the independent test solution. A different plate was used as a negative control, containing 24 eggs in the growing medium. Embryos were examined at 24, 48, 72, 96, and 120 h after treatment under a dissection microscope (Leica S6E, Germany). Four aspects of embryo death were observed, like Malafaia et al. (2020): 1) embryo survival percentage, 2) Heartbeat count, 3) body length and 4) hatchability percentage.

2.8. Statistical analysis

The death rate was calculated after 24 h. Probit analysis was used to determine their LC50 and LC90, Chi-square values, lower and upper confidence limits, and other statistics at 95% intervals (Finney, 1971). They were using the SPSS 16 version software for data analysis. Each experiment was tested three times. Parametric data are presented by the mean ± standard deviation, whereas non-parametric data are presented by the median and interquartile range.

3. Results

3.1. Characterization of biosynthesized silver nanoparticles

3.1.1. UV–vis spectroscopy

One of the most used techniques for characterizing nanoparticle formations is UV–visible spectroscopy. Visual observation was used to identify the color of the solution of $AgNO_3$ and *E. viscosus* leaf extract. The synthesis of Ag-NPs is shown in (Fig. 1A–C). The suspension color shifted from green to ash within 2 h. Aqueous leaf extract from *E. viscosus* absent $AgNO_3$ did not indicate any color change. The color of the extract changed from green to ash within 2 h, revealing the reduction of silver ions. The reduction of silver ions and synthesis of Ag-NPs were measured after 24 h using UV–vis spectrum at wavelengths ranging from 300 to 700 nm, which showed the highest peak at 435 nm gradually (Fig. 1D).

From the optical absorption spectra, the direct optical band gap was measured using

$$(\alpha h\nu)^n = A\ (h\nu - E_g)$$

Where E_g is the energy gap, α is the absorption coefficient, h is Planck's constant, ν is the frequency of light, A is the constant of proportionality, and n = 2 for direct band gap energy. From the plots (Fig. 1E), band gap energy is found to be 2.30 eV for as-prepared 24 h aging time respectively. The obtained band gap value confirmed that synthesized AgNPs are semiconducting, which matches with the previously reported silver nanoparticles (Chandhru et al., 2022).

3.1.2. FT-IR analysis of biosynthesized Ag-NPs

FT-IR spectroscopy was performed to evaluate the coating of plant extract on produced AgNPs. The hydroxyl group O–H shifting at 3910 cm^{-1}, the main amine N–H bond stretching at 3446 cm^{-1}, and the alkanes with various functional groups moving at 2932 cm^{-1} spectra are all depicted in the FT-IR spectrum of *E. viscosus* (Fig. 2A). The absorption peaks 2112 cm^{--1} are assigned due to the C═O stretch of carbonyls. The IR peak at 1733 cm^{-1} was associated with transaction ordered C–N bond of protein. Another similar peak, 1642 cm^{-1}, was assigned to the wagging vibration of the C–H bond of alkyl halides. The C–O stretch of carboxylic acid was observed at 1018 cm^{-1}, which was linked to the

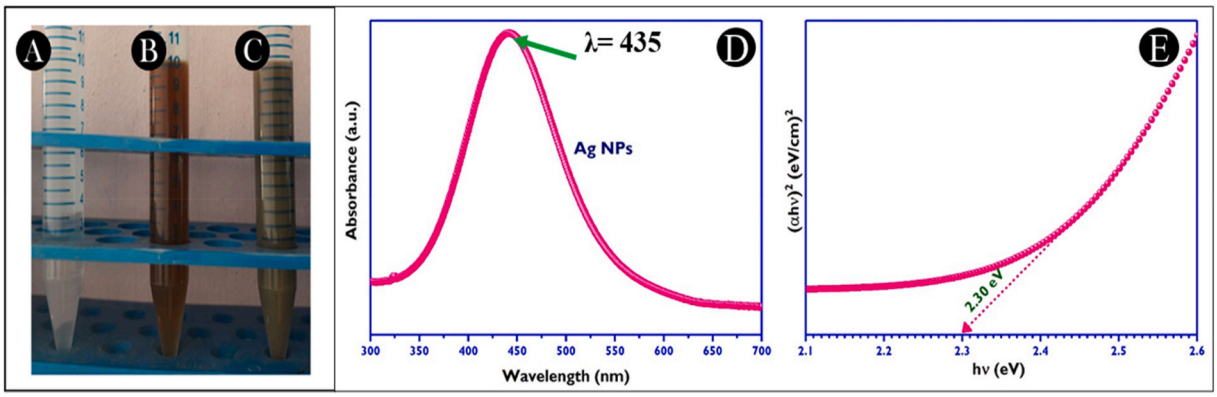

Fig. 1. (A) $AgNO_3$, (B) *E. viscosus* aqueous leaf extract, (C) biosynthesized Ag-NPs, (D) UV–visible spectra wavelength range of 300–700 nm recorded from aqueous *E. viscosus* leaf extract after 24 h with $AgNO_3$ solution (at 1 mM), (E) UV- band gap energy for Ag-NPs (2.30 eV).

amino acid residue, and the peptide had a strong ability to bind to metal nanoparticles. The peak at 945 cm^{-1} indicates the presence of C–Cl stretching medium vibrations of alkyl halides. Based on the FT-IR spectrum, the active biomolecules are carboxylic and amine groups responsible for reducing silver ions.

3.1.3. XRD analysis

It was determined that the particles were crystalline using X-ray diffraction. The XRD pattern showed some Bragg reflections with sharp peaks in the band of 2θ value ranging from 20 to 80°. The sharp peak at 27.6°, 32.6°, 46.1°, and 71.1° degrees corresponds to the 210, 111, 200, and 311 planes and confirms the silver's crystalline nature (Fig. 2B). The crystalline structure of the Ag-NPs produced by the reduction of Ag ions using *E. viscosus* leaf extract is indicated through X-ray diffraction. The Debye-Scherrer formula was used to determine the AgNP's crystalline phase with the support of a prominent intensity peak.

$$D = \frac{\lambda}{\beta \cos \theta} \tag{2}$$

where D is the mean crystallite size and 0.89 is Scherrer's constant. = The X-ray radiation's frequency (Cu K). = Full Width at Half-Maxima of the (1 0 1) plane of Ag-NPs. Bragg's angle of diffraction is equal to. The (1 0 1) strong plane's computed average crystallographic size was 14.8 nm.

3.1.4. TEM and EDX analysis

TEM micrographs show the size and shape of the biosynthesized Ag-NPs (Fig. 3A). Fig. 3B shows a histogram of the particle size distribution that the particles roughly exhibited a spherical shape ranging from 2 to 13 nm with an average size of 13 nm, which were readily redispersed in water. The produced AgNPs' elemental contents were examined via EDX in connection with HR-TEM, and the potential peaks were located between 1.741 and 10.430 keV, confirming the existence of Ag with an atomic percentage of 24.30% and a weight percentage of about 54.39%, respectively (Fig. 3C). Carbon and oxygen were also detected in the spectrum, which was associated with organic constituents of the leaf extract on the surface of Ag NPs.

3.1.5. Photocatalytic activity

The degradation of MB and CV dyes in the presence of sunlight was used to test the fabricated Ag-NPs' photocatalytic activity. The progressive transformation of the relevant color into a dye solution without color enabled for the visual observation of dye degradation. The photocatalytic decomposition of MB and CV dyes by biosynthesized Ag-NPs is demonstrated in Fig. 4, which displays the absorption spectra evaluated in the aqueous solution at various time intervals under the influence of Ag-NPs. With an increase in exposure time, the primary absorption peak at 595 nm steadily lowered, showing photocatalytic degradation of both dyes. The process stopped in the absence of the nano-catalyst (control). When exposed to sunlight for the first 20 min, degradation was observed at 19% and 21%. However, as photoperiod duration increased, the degradation efficiency of both the MB and CV of dye also grew, reaching a maximum at 180 min, which was 90% and 94%, as displayed in Fig. 4C and D. The primary active elements in the photocatalytic oxidation degradation of dye are gaps, superoxide anion radical, and hydroxide ions (Ravichandran et al., 2019). The photocatalytic investigations showed that these Ag-NPs are effective at destroying MB and CV when exposed to sunlight As an outcome, they can be used in textile and wastewater treatment processes.

The possible mechanism for the Ag NPs photodegradation of methylene blue (MB) and crystal violet (CV) dyes were proposed in Fig. 5. In the case of the Ag NPs under solar light irradiation, the photogeneration of electron–hole pairs on the surface of the Ag NPs occurs because of the Surface Plasmon Resonance (SPR) phenomena. Considering the fact that the reaction happens only on the surface of the nanoparticles, the electrons are promoted from the valence band (VB) to the conduction band (CB), leaving holes in the (h^+_{VB}) VB and conduction electron (e^-_{CB}) in the CB (Ansari et al., 2015). These photogenerated species leads to degradation of MB and CV in the reaction mixture by generating some highly reactive radicals (Eq. (1)). The e^-_{CB} by reacting with surface adsorbed dissolved oxygen (O_2) to form superoxide radical anions $(O_2^{\bullet -})$ (Eq. (2)). At the same time the photogenerated holes h^+_{VB} by reacting with surface adsorbed hydroxyl ions to form highly reactive hydroxyl radical $(HO^{\bullet})$ (Eq. (3) and (4)). Furthermore, $O_2^{\bullet -}$ also reacts with water molecule and finally produces $HO^{\bullet}$ and hydroperoxyl radical $(HO_2^{\bullet})$ (Eq. (5) and (6)) (Thamer and Murad, 2020). These highly oxidative species are play the key role in the photocatalytic degradation of MB dye like carbon dioxide (CO_2) and water (H_2O) and other degraded products (Eq. (7)). Based on the above mentioned arguments, it can be concluded that the Ag NPs exhibit enhanced photocatalytic activity due to the synergistic effects of the SPR phenomena of the Ag NPs.

$$Ag\ NPs + h\nu \rightarrow Ag\ NPs\ \left(e^-_{CB} + h^+_{VB}\right) \tag{1a}$$

$$O_2 + e^-_{CB} \rightarrow O_2^{\bullet -} \tag{2a}$$

$$H_2O + h^+_{VB} \rightarrow HO^{\bullet} + H^+ \tag{3}$$

$$HO^{\bullet} + HO^{\bullet} \rightarrow H_2O_2 \tag{4}$$

$$H_2O_2 + O_2^{\bullet -} \rightarrow HO^{\bullet} + HO^- + O_2 \tag{5}$$

$$H_2O_2 + e^- \rightarrow HO^{\bullet} + HO^- \tag{6}$$

$$Ag\ NPs\ \left(O_2^{\bullet -}, HO^{\bullet}, h^+_{VB}\ or\ HO_2^{\bullet}\right) \rightarrow Degraded\ Products \tag{7}$$

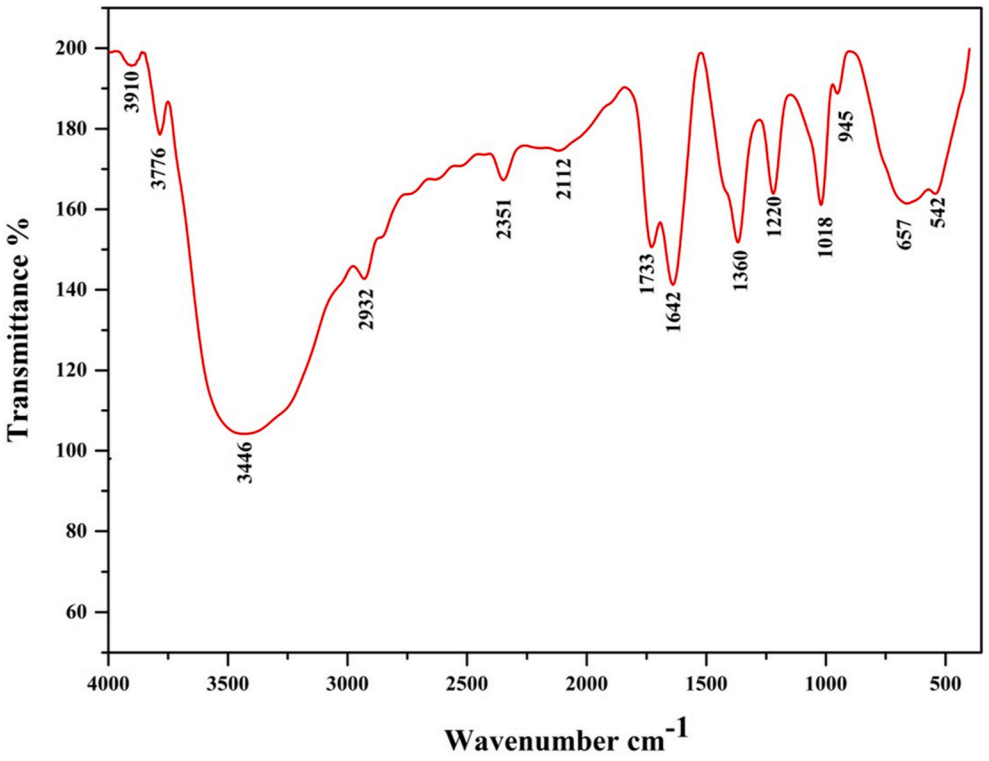

A. FT-IR spectrum synthesized Ag-NPs.

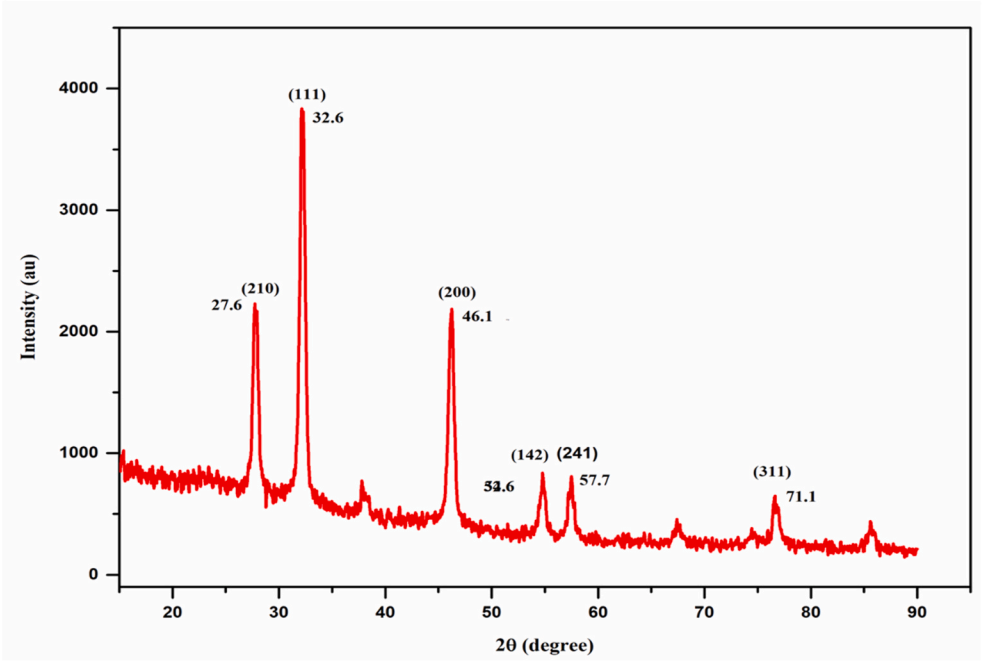

B. XRD spectra of synthesized Ag-NPs from *E. viscosus*.

Fig. 2. **A**. FT-IR spectrum synthesized Ag-NPs. **B**. XRD spectra of synthesized Ag-NPs from *E. viscosus*.

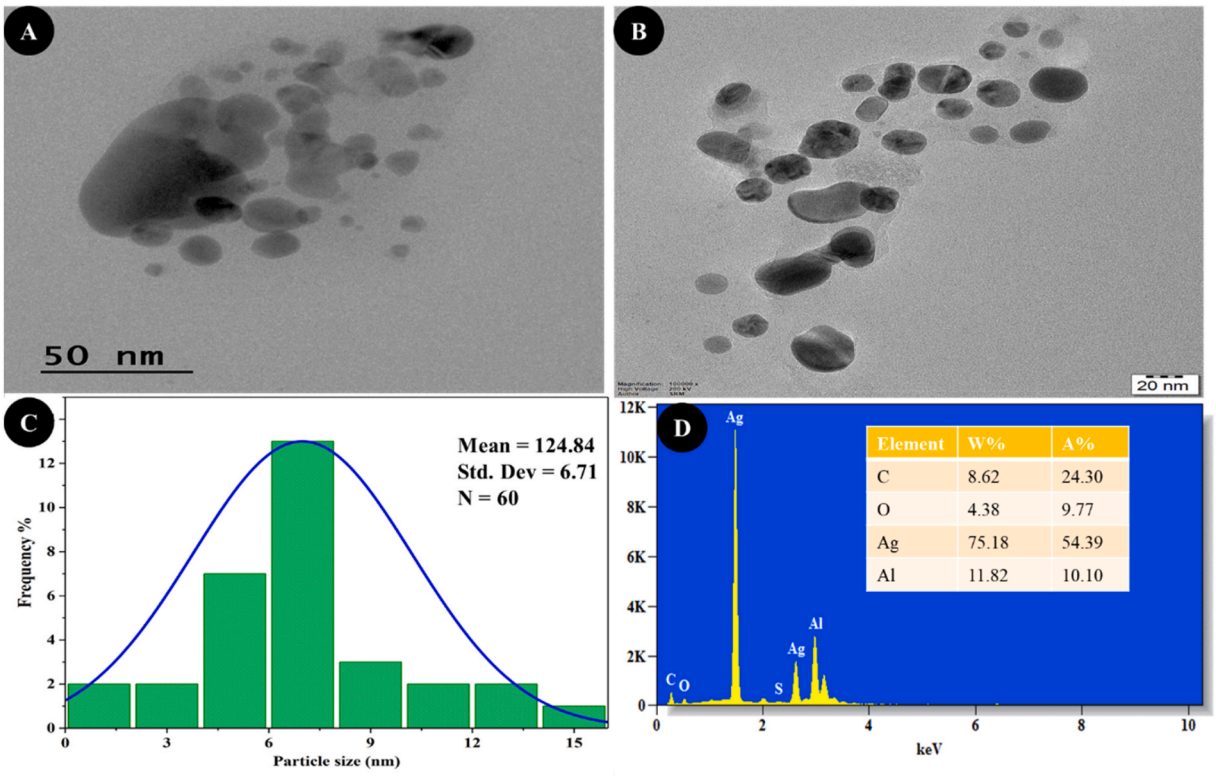

Fig. 3. (A–B) TEM images, (C) histogram representing the number-based distribution of the mean core diameter of the Ag-NPs (Scale bar: 50 nm), and (D) EDAX spectrum of biosynthesized Ag-NPs.

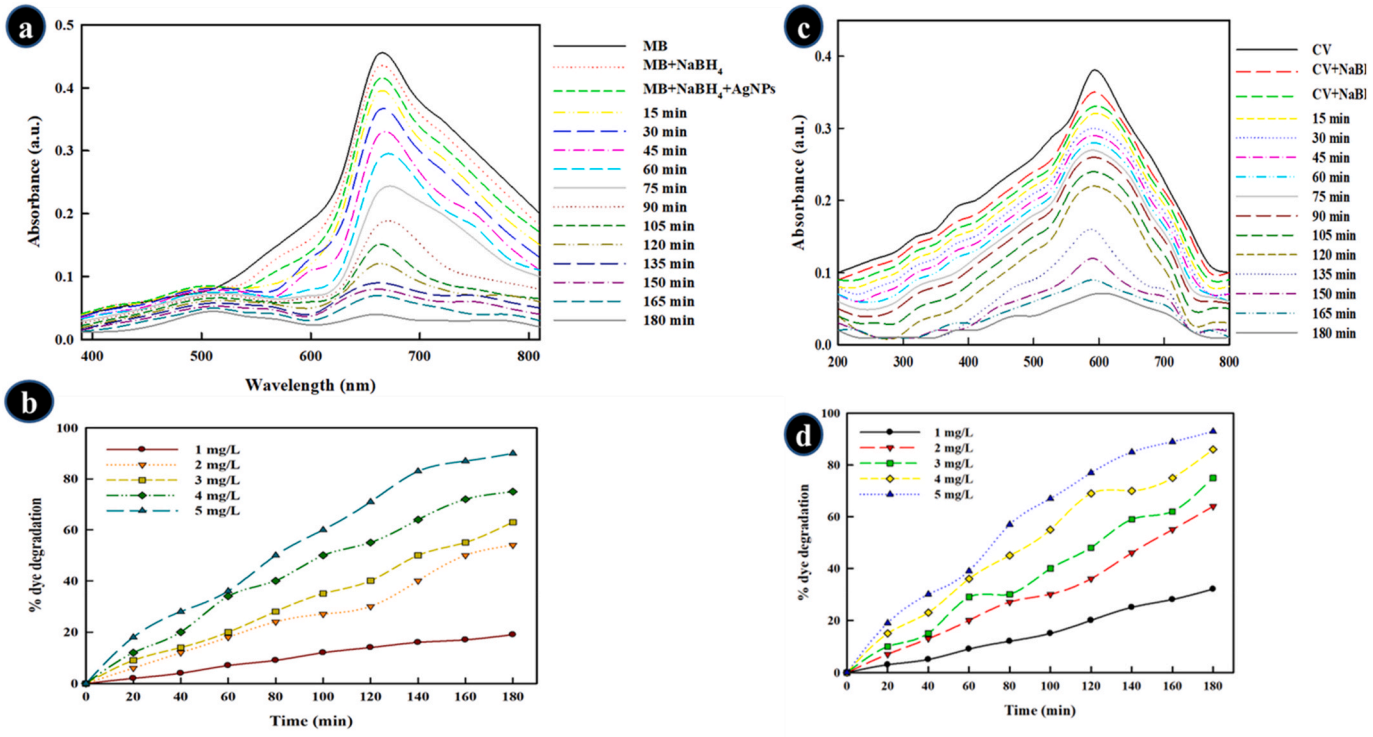

Fig. 4. Absorbance spectra of (**a**) methylene blue (MB) and (**c**) crystal violet dyes (CV) in the presence of synthesized Ag-NPs. Percentage of (**b**) MB and (**d**) dye degradation under sunlight irradiation. (For interpretation of the references to color in this figure legend, the reader is referred to the Web version of this article.)

3.1.6. Stability of Ag-NPs

The catalysts lifetime is an important parameter of the photocatalytic process because its use for longer period of time leads to a significant cost reduction of the treatment. For this reason, the catalyst was recycled which showed a drop in efficiency from 90% (1st cycle) to 94% (3rd

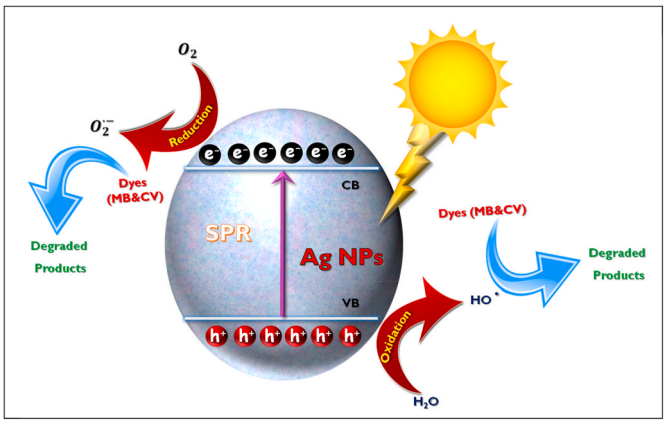

Fig. 5. Proposed photocatalytic degradation mechanism of MB and CV using Ag-NPs.

cycle) for both MB and CV dyes as shown in Fig. 6. These results indicated that Ag-NPs catalyst remained effective and reusable under solar light.

3.2. Antibacterial activity

Regarding the microbial assay, Fig. 7A–B illustrate Petri plate photographs used in the agar well diffusion test (with the inhibition zones) allowed monitoring of the antimicrobial activity of the biosynthesized AgNPs and other treatments against the *S. aureus* and *E. coli*, respectively. As seen in Fig. 7C–D, except for the "negative control" group, all treatments exhibited antimicrobial actions against the evaluated microorganisms. For *S. aureus*, we observed that biosynthesized Ag-NPs up to 100 μg/mL showed antimicrobial activity superior to that exhibited by NPs at a concentration of 50 μg/mL (an increase of 80.6%) and to that induced by chloramphenicol (positive control, up to 100 μg/mL), whose increase was >22%. On the other hand, the zone inhibition diameter values recorded for *E. coli* reveal similar antimicrobial activity between the biosynthesized Ag-NPs and aqueous extract groups (for both concentrations tested). More expressive antimicrobial activity of chloramphenicol (Fig. 7B). Therefore, these results reveal the potential antimicrobial activity of biosynthesized Ag-NPs (up to 100 μg/mL) activity against Gram-positive bacteria.

3.3. Antioxidant activity

The results of the DPPH radical scavenging activity and the reducing power assays of biosynthesized Ag-NPs are shown in Fig. 8A–B, respectively. In both assays, the Ag-NPs showed higher antioxidant capacity than the aqueous extract of *E. viscosus* at all concentrations tested. The antioxidant activity of Ag-NPs was, on average, higher than 58% about the treatment with the aqueous extract. Furthermore, we noticed that the antioxidant action of biosynthesized Ag-NPs, as well as for the aqueous extract and ascorbic acid, was concentration-dependent in both assays (Fig. 9A–B).

3.4. Larvicidal activity

Regarding larvicidal activity, we observed the interaction between the factors "larval development stage" and "concentrations" in the mortality rate of *Ae. aegypti* larvae induced by biosynthesized (Fig. 10A). For larvae of all stages evaluated (first to fourth instar stage) (Fig. 10B), we also observed a concentration-dependent effect (Fig. 10C). While for the larvae of the first, second, and third instar stages, an average mortality rate of 85.2% was observed in animals exposed to Ag-NPs (to 250 μg/mL); in fourth instar larvae, the highest concentration of NPs induced the death of more than 90% of the animals (Table 1). The LC_{50} and LC_{90} results were written as follows: LC_{50} = 9.629, 6.969, 4.509, and 4.009 μg/mL; LC_{90} = 12.420, 8.374, 7.401, and 6.626 μg/mL, respectively (Table 1). No death could be documented in the control group.

3.5. Histopathological analysis

Histopathological investigations of 4th instar *Ae. aegypti* larvae exposed to biosynthesized Ag-NPs (at 250 μg/mL) displayed structural changes in the digestive system, the midgut, and the cortex. These changes included hyperplasia of gut epithelial cells, a broken brush border, ruptured membranes, and the presence of cytoplasmic clusters (Fig. 11A). Control (untreated) larvae had a single layer of gastric cells with well-developed brush surfaces, cell membranes, and cytoplasm areas in the midgut cells (Fig. 11B).

3.6. Toxicity studies on zebrafish embryo

The toxicity evaluation of biosynthesized Ag-NPs to zebrafish embryos *in vivo* revealed a significant impact of the nanomaterials only at concentrations of 500 and 1000 μg/L. In these groups, we observed a significant reduction in the hatching rate of eggs (Fig. 12A), a negative impact on the growth of the animals (inferred by body length) (Fig. 12B), as well as changes in the heartbeat (Fig. 12C). Furthermore, zebrafish embryos exposed to Ag-NPs exceeding 500 μg/mL exhibited visible abnormalities, such as a bent spine, egg aggregation, tail deformation, and hatching delay between 8 and 120 h post fertilization (Fig. 12). Such abnormalities may explain the low survival rate of animals in groups exposed to Ag-NPs at 500 and 1000 μg/mL compared to the control group and other NP concentrations (Figs. 13 and 14).

4. Discussion

Various attempts to synthesize silver, gold, titanium, and zinc oxide

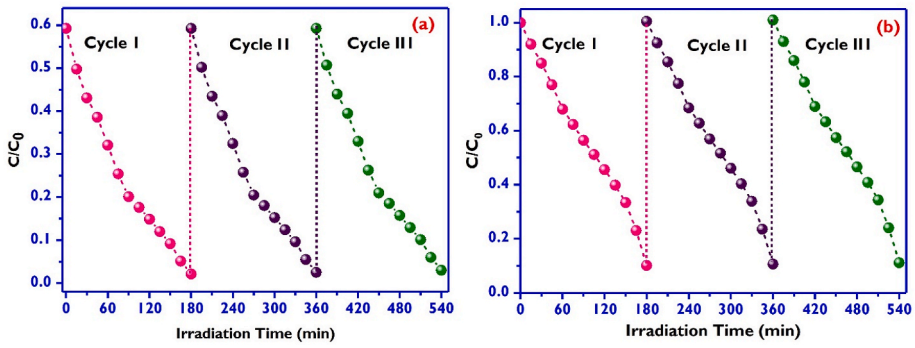

Fig. 6. Recycling and stability tests of Ag-NPs for degradation of (a) MB and (b) CV dyes.

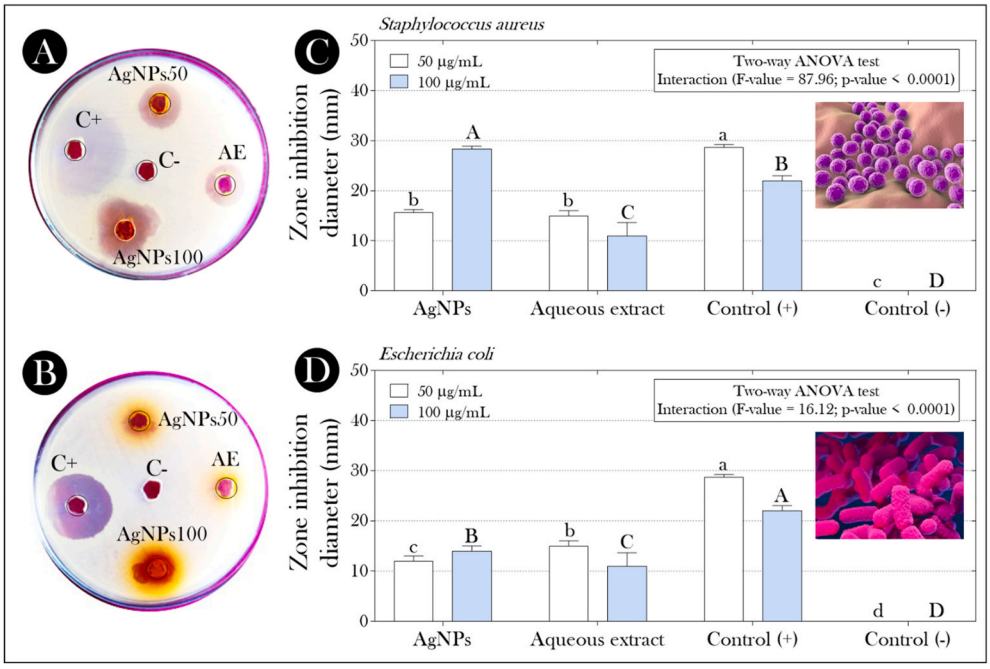

Fig. 7. Antibacterial activity of biosynthesized Ag-NPs and other treatments against (A) *S. aureus* and (B) *E. coli*, and (C–D) zone inhibition diameter referring to the respective microorganisms. Note: C+: positive control (Chloramphenicol); C-: negative control; Ag-NPs50: biosynthesized Ag-NPs at 50 µg/mL; Ag-NPs100: biosynthesized Ag-NPs at 100 µg/mL, and AE: aqueous extract of *E. viscosus*. Distinct lowercase letters and uppercase letters indicate significant differences between the zone inhibition value referents to the different treatments at 50 and 100 µg/mL, respectively.

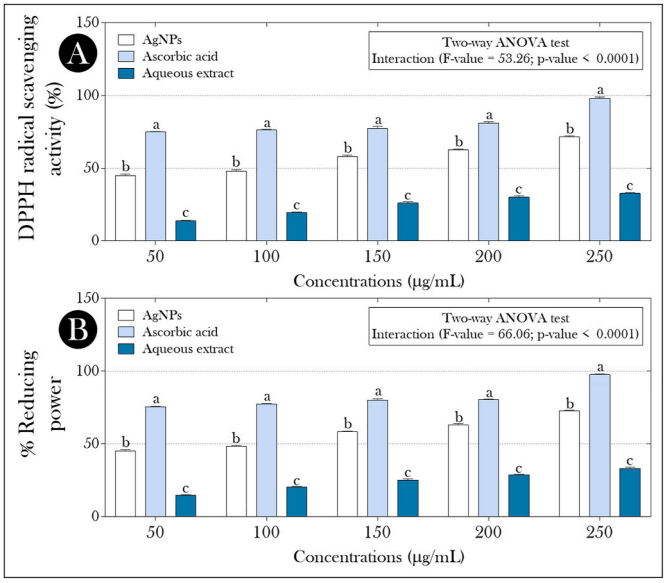

Fig. 8. (A) DPPH radical scavenging activity and (B) reducing power of biosynthesized Ag-NPs from *E. viscosus*. Bars indicate the mean +standard deviation. Summaries of statistical analyzes are displayed at the top of the graphs. Distinct lowercase letters indicate significant differences between the antioxidant capacity of treatments within the same concentration tested.

NPs, etc., utilizing bio-based components, including fungi, bacteria, algae, protein, plants, and others, resulting from the increasing influence of green manufacturing techniques (Srikar et al., 2016). NPs are used in many different biological disciplines. Hence new research is being done on their synthesis utilizing different materials in distinct shapes and sizes, namely platinum, palladium, silver, and gold. Ag is an excellent metal that is best for use in biological, medical, and systems, as well as biological ones (Tiri et al., 2022). The present study mainly focused on the eco-friendly nano-synthetic approach to biomedical Ag-NPs. Color changes, UV–Vis, FTIR spectroscopic measurements, EDAX, and TEM analysis are characterized by biosynthesized Ag-NPs. Reducing Ag + ions to Ag is necessary for the synthesis of $AgNO_3$. The ingredients of leaf extract reduce agents in the production of silver NPs. The present study has effectively developed a green synthetic approach for producing silver nanoparticles using aqueous *E. viscosus* leaf extract. The first sign of the production of silver NPs is the investigation's shift in the color of the leaf extract mixture from greenish yellow to dark brown. This color change was observed after adding a solution of silver nitrate to the aqueous extract solution of *Nigella sativa* and *Hibiscus sabdariffa* (Mares-Briones et al., 2019; Karimi et al., 2022). A surface plasmon resonance (SPR) absorption band was detected in the UV–vis spectrum between 390 and 530 nm, which is typical for metal Ag-NPs (Oliver et al., 2018). The SPR of silver NPs was observed at 435 nm. Similarly, Ntoumba et al. (2019) showed that the UV–vis spectroscopy at 430 nm detected the *Psidium guajava-produced* Ag-NPs. Recently, Nawabjohn et al. (2021) reported that the *Cassia tora* seed extract-derived Ag-NPs displayed a strong band at 423 nm in UV–vis spectroscopy.

The FTIR measurement helps to determine potential biomolecules that bind and effectively stabilize metal nanoparticles. The current data clearly demonstrated the role of polyphenols, carboxyl, amine groups, and amino acid residues in forming Ag-NPs. According to a previous study by Loi et al. (2020), plants have bioactive components such as saponin, quinone, protein, phenols, and flavonoids that efficiently attach to silver NPs via either amine groups or cysteine remains in the proteins, stabilizing the Ag-NPs in the process. Diana and Mathew's (2022) research shows that the efficient groups C═O, O–H, and N–H in amino acids and proteins have a strong affinity for binding to metals to make highly stable nanoparticles (NPs). This demonstrates that the terpenoids, which have amine groups, alcohols, carboxylic acids, and chemical bonding in their alkanes, are encircled by many proteins and bioactive compounds, mainly the extract-derived Ag-NPs. Another study has assigned that the peak at 2351cm-1 is due to –C═C- alkynes stretching. This signifies that secondary plant metabolites like flavonoids, which are water soluble, may cap silver nanoparticles. The current study shows that, in the absence of additional potent ligating agents in adequate concentration, flavanones or terpenoids adsorbed on the surface of metal nanoparticles, potentially through interaction through carbonyl groups or π-electrons. Earlier, Kaur et al. (2022) hypothesized that the terpenoids may contribute to the reduction of metal ions by oxidizing the molecules' aldehydic groups to carboxylic acids while

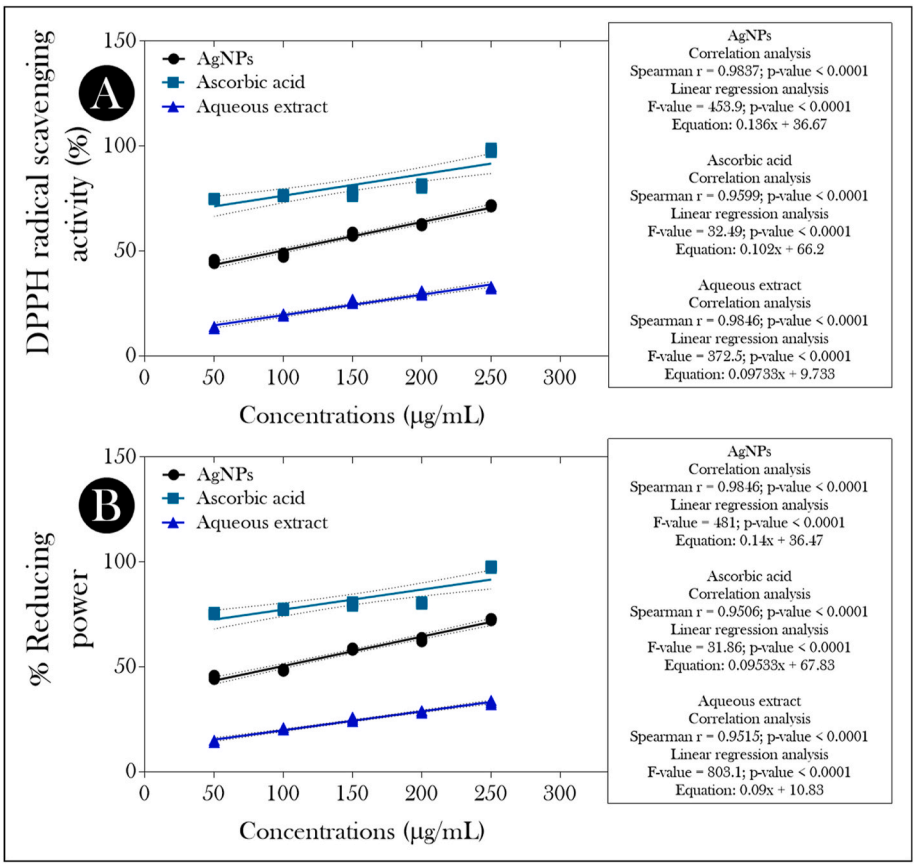

Fig. 9. Análise de correlação entre as concentrações of biosynhesized Ag-NPs and atividade antioxidante observada pelo (A) DPPH and (B) reducing power assays.

investigating the production of metal oxide nanoparticles by various plant leaf extracts. Generally, the bio ingredients that maintain Ag-NPs interact with metallic ions through these amino acids. This action leads Ag to be converted to nanoparticle form. The carboxyl groups of amino acids and proteins can connect metals and inhibit their agglomeration, according to Elumalai et al. (2017). Interestingly, it has been suggested that biological materials like nucleic acids can mediate the production of Ag-NPs by serving as reducing agents (Ahmad et al., 2019).

The XRD spectrum of the materials must be studied to determine the specific nature of the silver particles synthesized. The XRD spectrum has demonstrated the face-cantered cubic (fcc) structure and crystalline size of the synthesized Ag-NPs. Present results, XRD analysis displayed strong peaks agreeing to (111), (200), (220), and (311) Bragg's reflection built on the structure of silver NPs. Similar results in silver NPs are synthesized using *Camellia sinensis* extract (Gol et al., 2020). Fascinatingly, Zhang et al. (2020) analyzed the *Flammulina velutipes* Ag-NPs and found that they displayed XRD peaks at 2θ values of 38.2°, 44.3°, 64.7°, and 77.9°. Transmission electron microscopy (TEM) was used to determine the surface morphology of the material and provide information/data on Ag-NPs. The TEM images clearly display the oval and spherical-like structure with irregular arrangements. The synthesized NPs were confirmed to have a diameter of around 2–13 nm and to be globular in shape. Similar findings indicate that the Ag-NPs from *Bauhinia purpurea* is primarily spherical, with an average size of 16.8 nm and a range of 7.5–25 nm (Chinnappan et al., 2018). EDAX spectra provide qualitative and quantitative data about the sample's elemental content. The EDAX spectra allow us to conclude that the sample lacks other substances, such as impurities or adducts. The number of elements present in the synthesized samples is associated with the intensity of the spectra. The energy dispersive spectroscopy (EDAX) shows a high signal for Ag, whereas minor signs have been seen for carbon, chloride, and oxygen. The EDAX spectrum of Ag-NPs shows clear peaks of Ag, C, and O with a weight percentage of 54%, 24%, and 9%, respectively (Renuka et al., 2021). Similarly, Hemlata et al. (2020) investigation of *Cucumis prophetarum* aqueous extract-mediated manufactured silver nanoparticles demonstrated a high silver absorption peak at 3 keV due to silver being one of the main elements.

The antibacterial effects of Ag-NPs were investigated against human clinical pathogens using the well diffusion method. The outcomes of the *E. viscosus* synthesized Ag-NPs have effective antibacterial activity against *S. aureus* and moderate growth inhibition against *E. coli.* Silver's capability to inhibit bacterial growth has been known for decades (Dridi et al., 2022). Silver ions are highly effective against human pathogenic bacteria, even at minimal concentrations. The antibacterial activity of silver particles is influenced by particle size, in contrast to the bactericide impacts of silver ions. The minimal particles have higher antimicrobial action (Liao et al., 2019). Gram -ve bacteria *E. coli* observed the highest zone of inhibition at 15 mm in 100 µg of Ag-NPs. In the case of 50 µg/mL concentration, both strains had a small zone of inhibition less than 15 mm in diameter. Similar outcomes were found by Rizwana et al. (2022), which may be related to the Gram-negative bacteria's thinner cell walls, which are made up of a single layer of peptidoglycan. Gram + ve bacteria have thick cell walls of multiple layers of peptidoglycan, which impede Ag-NP transport and penetration (Miri et al., 2015; Yin et al., 2020). The silver metal ions produced by Ag-NPs contribute strongly to alteration in the structure of bacteria' membranes, which in turn impact the bacteria's membrane permeability to increase and ultimately lead to cell death (Zhao et al., 2022; Li et al., 2022). Ag + ion releases from Ag-NPs may affect biological macromolecules, including phospholipids, proteins, and nucleic acids, to be damaged, increasing the antibacterial potency of Ag-NPs (Taran et al., 2016). The formation of gaps or pores in the bacterial membrane or cell wall is probably triggered by an electrostatic interaction between the positive charge of Ag + ions and the negative charge of the bacterial cell wall (Alavi et al.,

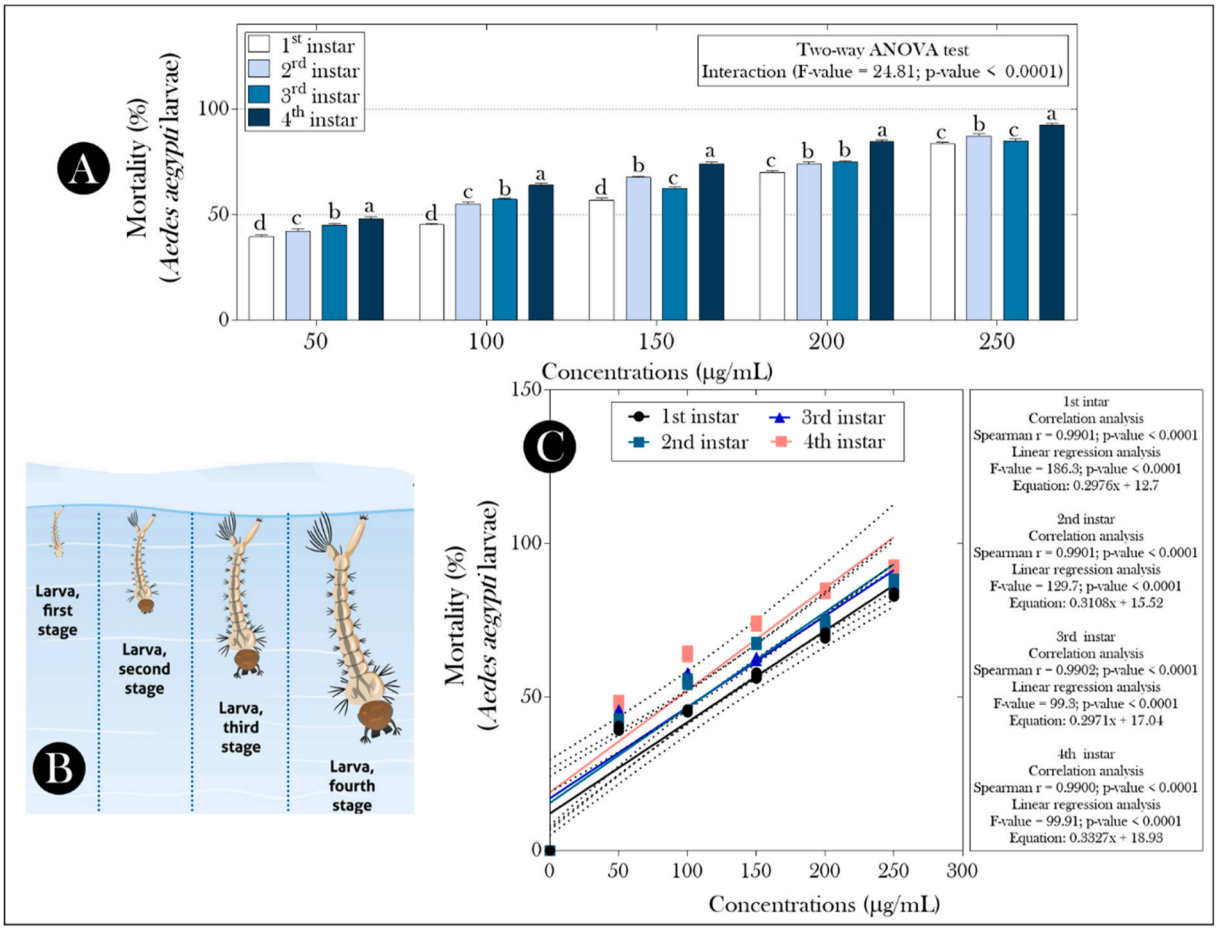

Fig. 10. (A) Mortality rate of *Ae. aegypti* larvae exposed to biosynthesized Ag-NPs at different concentrations and (B) representative images of different larval stages of *Ae. aegypti*. (C) Correction analysis between mortality rate and concentrations of Ag-NPs. In "A", bars indicate the mean +standard deviation. Summaries of statistics are displayed at the top or next to the graphs. Distinct lowercase letters indicate significant differences between larvae of different stages within the same concentration tested.

Table 1
Larvicidal activity (against *Ae. aegypti* larvae) of the synthesized Ag-NPs from *E. viscosus*.

Larval stages	Concentrations of biosynthesized AgNPs (µg/mL)	24-h mortality (%) ± SD[a]	LC_{50} (µg/mL) (LCL- UCL)	LC_{90} (µg/mL) (LCL- UCL)	χ^2 (df = 4)
1st instar	Control	0.0 ± 0.0	9.269 (2.281–13.643)	12.420 (4.478–19.054)	8.324*
	50	39.6 ± 0.5			
	100	45.3 ± 1.0			
	150	57.0 ± 1.0			
	200	70.0 ± 1.0			
	250	83.6 ± 0.5			
2nd instar	Control	0.0 ± 0.0	6.798 (3.916–13.954)	8.374 (5.256–17.715)	7.298*
	50	42.3 ± 0.5			
	100	55.0 ± 1.0			
	150	67.6 ± 0.5			
	200	74.0 ± 1.6			
	250	87.2 ± 0.5			
3rd instar	Control	0.0 ± 0.0	4.509 (2.981–10.514)	7.401 (3.240–14.520)	4.931*
	50	45.1 ± 1.0			
	100	57.30 ± 0.5			
	150	62.5 ± 0.5			
	200	75.0 ± 1.6			
	250	85.0 ± 1.3			
4th instar	Control	0.0 ± 0.0	4.009 (2.505–9.676)	6.626 (3.102–12.163)	4.210*
	50	48.0 ± 1.0			
	100	64.0 ± 1.0			
	150	74.0 ± 1.0			
	200	85.5 ± 1.5			
	250	92.5 ± 1.5			

Note: Control- Nil mortality, [a]Mean value of five replicates, *$p < 0.05$, level of significance. LC_{50} and LC_{90}: lethal concentration that kills 50% and 90% of the exposed larvae, UCL: upper confidence limit, LCL: lower confidence limit, χ^2: chi-square, *df*: degree of freedom.

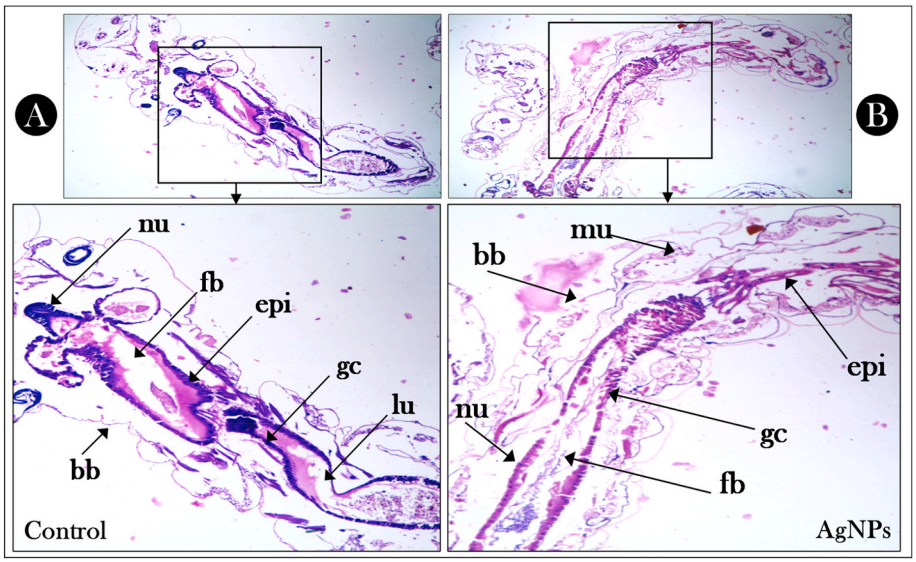

Fig. 11. Photomicrographs representative of histological profiles observed in the 4th instar of *Ae. aegypti* larvae – (A) unexposed and (B) exposed to biosynthesized Ag-NPs (at 250 μg/mL). Note: epi: gut epithelium, nu: intact neuropile, gc: damaged gastric enteric) caeca, bb: brush border, fb: food bolus, lu: gut lumen.

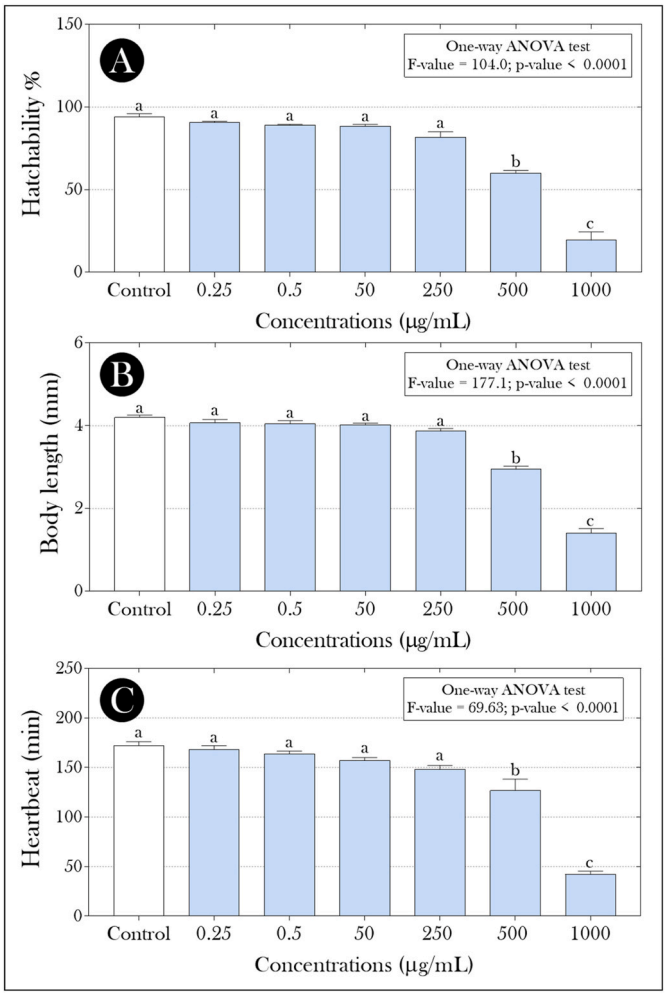

Fig. 12. (A) Hatchability, (B) body length, and (C) heartbeat of zebrafish (*Danio rerio*) embryos exposed or unexposed to biosynthesized Ag-NPs in different concentrations. Bars indicate the mean +standard deviation. Summaries of statistics are displayed at the top of the graphs. Distinct lowercase letters indicate significant differences between the experimental groups.

2019; Maleki et al., 2021).

Silver nanoparticles produced from a plant extract have also been studied for their capacity to neutralize free radicals. Ag-NPs produced from the aqueous leaf extract of *E. viscosus* demonstrated greater antioxidant activity in the DPPH assay than the aqueous leaf extract, despite the leaf extract's higher phenol concentration. These results, which are in good agreement with *Pantoea anthophila* synthesized silver NPs also exhibited antioxidant activity, which was determined using DPPH radical scavenging assays (Nirmala and Sridevi, 2021). The results showed that increasing concentrations of both aqueous extract and Ag-NPs enhanced their antioxidant potential. However, compared to ascorbic acid/reference, aqueous and Ag-NPs produced slightly less activity. Similarly, Jahan et al. (2021) reported that the *Malus domestica* and *Cuminum cyminum*-derived silver nanoparticles had higher antioxidant activity in DPPH and ABTS. Rajkumar and Sundar (2022) recently observed that the fabricated silver nanoparticles from *Persea americana* seed extract exhibited powerful DPPH free radical scavenging ability.

To the best of our scientific knowledge, the present study's first investigation on the biosynthesized *E. viscosus* Ag-NPs was evaluated for its efficacy against 1st to 4th instar larvae of *Ae. aegypti*. The larvae were exposed to various concentrations (50–250 μg/mL) of silver nanoparticles, and 4.09 μg/mL was recorded as the LC_{50} value. Rajput et al. (2020) revealed the bio-larvicidal activity of Ag-NPs against targeted larvae. Based on their outcomes, the maximum larval death was observed in the synthesized Ag-NPs against 1st to 4th instar larvae LC_{50} (9.62, 6.96, 4.59, 4.00 μg/mL, respectively), LC_{90} (12.42, 8.37, 7.40 and 6.62 μg/mL). In the present investigation, the biosynthesized Ag-NPs from the leaf extract of *E. viscosus* noticed effective larvicidal activity against *Ae. aegypti*. Therefore, the larvicidal activity of silver NPs may be influenced by the inactivation of phosphorous/sulfur-containing proteins or DNA, which consequently results in the dissociation of organelles and enzymes and shrinks cellular membrane fluidity and ATP synthesis, ultimately due to the destruction of cellular function and cell death (Mondal et al., 2022). Nanomaterials are employed in various pharmaceutical, industrial, and biomedical applications, and their size and shape are essential (Sap-Iam et al., 2010). Satsangi and Preet (2021) recently reported that the *Nyctanthes arbortristis* synthesized Ag-NPs exhibited the highest efficacy against three targeted mosquito vectors. Ag-NPs can attach to substances like DNA that contain sulfur or phosphorus, denature those substances or inhibit the activity of certain enzymes, and therefore reduce the membrane's permeability. The larval membrane is thus destroyed due to the changing proton motive force

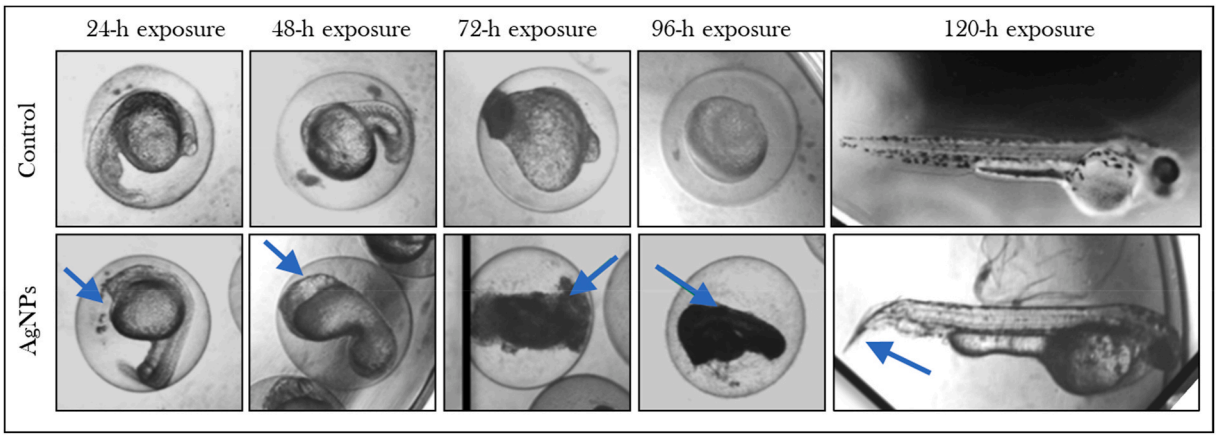

Fig. 13. Microscopic images showing morphological changes in zebrafish (*Danio rerio*) embryos between (A) control and (B) exposed to biosynthesized Ag-NPs (1000 μg/mL) at 24, 48, 72, and 96 hpf time intervals. Blue arrow noticed malformations. (For interpretation of the references to color in this figure legend, the reader is referred to the Web version of this article.)

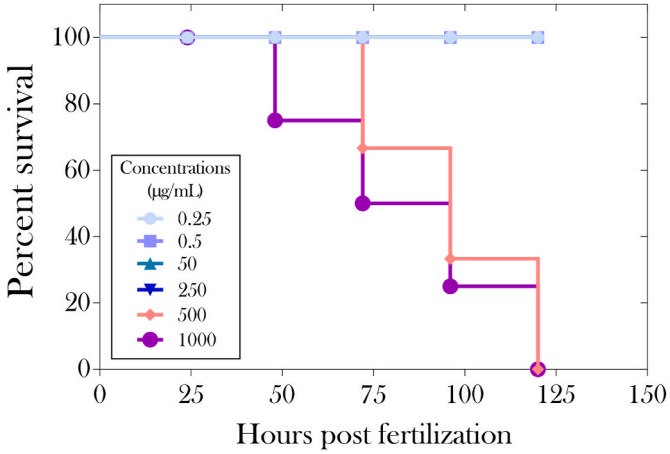

Fig. 14. Percentual survival of zebrafish (*Danio rerio*) larvae exposed or unexposed to synthesized Ag-NPs at different hours post fertilization time intervals.

(Barua et al., 2016). Al-Hakimi et al. (2022) recently reported that the *Nerium oleander*-mediated synthesis of Ag and Au nanoparticles evaluated larvicidal activity against *Ae. aegypti* with the least LC_{50}, 36.07, and 46.64, respectively.

The photocatalytic action is highly dependent on the crystal lattice, shape, and size of the metal NPs, as well as sunlight-induced color degradation (Mechouche et al., 2022; Balamurugan et al., 2022). One of the fundamental techniques for treating dye effluent is photocatalysis. After radiation exposure, electrons from the valence band to the conduction band generate electron-hole pairs. The dye was converted entirely into nonhazardous compounds due to the oxidizing effects of the resultant hydroxyl radical (CO_2, H_2O, etc.) Marimuthu et al. (2020). A different amount of Ag-NPs was tested with high quantities of methylene blue and crystal violet. The greatest absorption rate in the present research was found at 595 nm for methylene blue and 595 nm for crystal violet. Similarly, Madhu et al. (2022) investigated that the *Praecitrullus fistulosus* fruit extract produced Ag-NPs exhibit strong photocatalytic activity against methylene blue and trypan blue under sunlight irradiation. This graph shows the relationship between time and dye concentration at various periods after 3 h of exposure to visible light. Periyasami et al. (2022) recently investigated that the *Euphorbia granulata* synthesized Ag-NPs showed promising catalytic properties against methylene blue and methylene orange organic dyes. Likewise, Kumar et al. (2013) have investigated the degradation of methyl orange dye using Ag-NPs produced from *Ulva lactua*. Additionally, many phytochemicals found in plant extracts and even on the surfaces of nanoparticles work as catalysts to boost photocatalytic activity, resulting in a more efficient breakdown of dye components. *Astragalus flavesces*-mediated produced Ag-NPs were tested using methylene blue under solar light irradiation, and 69% degradation was seen after 24 h, according to Sahin Yaglioglu et al. (2022).

The most widely used vertebrate model animal, zebrafish, is found in freshwater ponds, creeks, and lakes. It is one of the organisms used in ecotoxicity tests which is the most delicate (Nagalingam et al., 2018). The zebrafish is an ideal animal model for examining toxic substances' impact on the visual system's growth. To measure the deleterious effects on zebrafish embryos, using varying concentrations of silver NPs were conducted. To assess the potential toxicity of zebrafish (*Danio rerio*) embryo exposure to various concentrations of biogenically produced Ag-NPs by measuring mortality and hatching rate (0.25–500 μg/mL and 1 mg/mL). At a higher concentration of 1 mg/mL, a decrease in the heartbeat, body length, and hatching percentage is observed for the Ag-NPs.

Similarly, Qiang et al. (2020) have observed that Ag-NPs exposed to zebrafish embryos exhibited decreased body length compared to untreated groups. The biogenic-produced Ag-NPs were provided to *Danio rerio* at a concentration of 500 μg/mL, and no harmful effects were seen. The current observations supported past studies' findings that exposure to Ag-NPs would harm fish eggs and provide health risks at greater concentrations (Lee et al., 2022). The schematic for the entire production of biogenic Ag-NPs, their characterization, and capping confirmation utilizing distinct approaches in combination with *E. viscosus* aqueous extract is presented in Fig. 15.

5. Conclusion

Here, it is first reported that *E. viscous* leaf extract was used to generate Ag-NPs successfully. The FTIR results demonstrated that the leaf extract has a good prospect for use as an agent for stabilizing and capping Ag-NPs. The structure of the Ag NPs was determined using UV–Visible, FTIR, XRD, TEM, and EDAX spectra. TEM photographs showed that most particle sizes are between 2 and 13 nm. The higher larvicidal activity (90%) was obtained at a maximum concentration of Ag-NPs. Histological profiles were altered while treating with Ag-NPs at maximum doses. The findings of the antibacterial activity test reveal that Ag-NPs have a significant capacity to inhibit the growth of *S. aureus* and *E. coli*. Ag-NPs had an average antioxidant (DPPH and FRAP) activity of more than 58%. Furthermore, *in vivo* toxicity of fabricated Ag-NPs was efficiently evaluated using zebrafish embryos and larvae (*Danio*

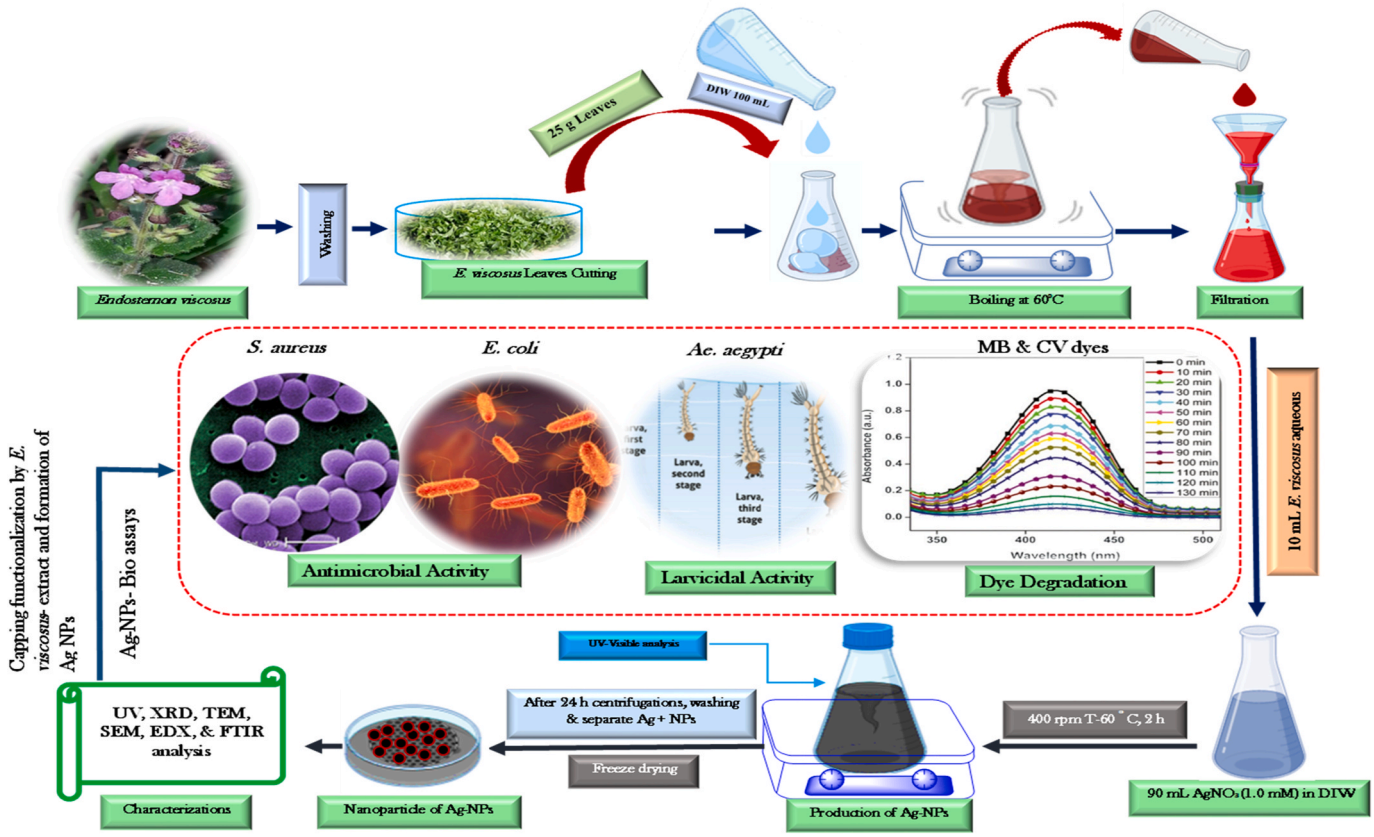

Fig. 15. Schematic for making biogenic AgNPs, characterization, and capping determination using various procedures in combination with *E. viscosus* aqueous extract.

rerio) model various hours post-fertilization. Our outcomes exhibited that minimal concentrations of the Ag-NPs didn't display severe toxicity to the zebrafish embryos. As future investigative perspectives, we recommend expanding biomarkers of toxicity of biosynthesized Ag-NPs in *A. aegypti* mosquito larvae (e.g., genotoxic, mutagenic, molecular effects, etc.) and that assessments of the possible impact of NPs on adult individuals be performed. On the other hand, the potential use of biosynthesized Ag-NPs for pollutant remediation should encompass assessments that include pollutants, such as heavy metals, pesticides, and pharmaceuticals, commonly identified in domestic and industrial effluents. In future work, other NPs-based antibacterial materials can be synthesized using *E. viscosus,* and the effect on other bacteria can be analyzed. The Ag-NPs can be applied and developed as environmentally friendly and efficient nanocatalysts in wastewater treatment.

Author contribution statements

CR, KDJ, and CK: planned the research, conducted the experiments, shared chemicals, analyzed the tools, and wrote the manuscript. VM: conceptualization, methodology, and performed the embryotoxicity experiments. TC: evaluation of dye degradation work. CR, GM, and WP: writing, reviewing, and editing. All authors have read and decided on the published version of the manuscript.

Ethical aspects

The ethical guidelines for animal research were strictly followed during all experimental procedures. Laborious measures were taken to reduce the animals' distress and external causes of stress, pain, and discomfort. The number of animals used in the current investigation is within the range required to provide valid scientific data. This article doesn't cite any human studies by the authors.

Declaration of competing interest

The authors declare that they have no known competing financial interests or personal relationships that could have appeared to influence the work reported in this paper.

Data availability

Data will be made available on request.

Acknowledgements

The Council for Scientific and Industrial Research (CSIR), Government of India, New Delhi, is thanked for the released grant (Ref. Lr. 09/810 (0024)/2016-EMR-I) under the CSIR-SRF (Direct) Senior Research Fellowship. Leiden University partially supported this work. Furthermore, the authors thank the Goiano Federal Institute (IF Goiano/GO/Brazil) and the National Council for Scientific and Technological Development (CNPq/Brazil) for the financial support needed to conduct this research. Malafaia G. holds a productivity scholarship from CNPq (Proc. No. 308854/2021-7).

References

Abadi, B., Hosseinalipour, S., Nikzad, S., Pourshaikhali, S., Fathalipour-Rayeni, H., Shafiei, G., Forootanfar, H., 2022. Capping agents for selenium nanoparticles in biomedical applications. J. Cluster Sci. 1–22.

Abbott, W.S., 1925. A method of computing the effectiveness of an insecticide. J. Econ. Entomol. 18, 265–267.

Ahmad, S., Munir, S., Zeb, N., Ullah, A., Khan, B., Ali, J., Ali, S., 2019. Green nanotechnology: a review on green synthesis of silver nanoparticles—an eco-friendly approach. Int. J. Nanomed. 14, 5087.
Ahmad, W., Jaiswal, K.K., Soni, S., 2020. Green synthesis of titanium dioxide (TiO_2) nanoparticles by using *Mentha arvensis* leaves extract and its antimicrobial properties. Inorg. Nano-Metal. Chem. 50 (10), 1032–1038.
Akgul, H., Mohammed, F.S., Kına, E., Uysal, İ., Sevindik, M., Doğan, M., 2022. Total antioxidant and oxidant status and DPPH free radical activity of *Euphorbia eriophora*. Turkish J. Agri-Food Sci. Technol. 10 (2), 272–275.
Alavi, M., Karimi, N., Valadbeigi, T., 2019. Antibacterial, antibiofilm, antiquorum sensing, antimotility, and antioxidant activities of green fabricated Ag, Cu, TiO_2, ZnO, and Fe_3O_4 NPs via *Protoparmeliopsis muralis* lichen aqueous extract against multi-drug-resistant bacteria. ACS Biomater. Sci. Eng. 5 (9), 4228–4243.
Al-Hakimi, A.N., Abdulghani, M.A., Alhag, S.K., Aroua, L.M., Mahyoub, J.A., 2022. Larvicidal activity of leaf extract of *Nerium oleander* L. and its synthesized metallic nanomaterials on dengue vector, *Aedes aegypti*. Entomol. Res. 52 (3), 148–158.
Amarasinghe, L.D., Wickramarachchi, P.A.S.R., Aberathna, A.A.A.U., Sithara, W.S., De Silva, C.R., 2020. Comparative study on larvicidal activity of green synthesized silver nanoparticles and *Annona glabra* (Annonaceae) aqueous extract to control *Aedes aegypti* and *Aedes albopictus* (Diptera: Culicidae). Heliyon 6 (6), e04322.
Ansari, S.A., Khan, M.M., Ansari, M.O., Cho, M.H., 2015. Silver nanoparticles and defect-induced visible light photocatalytic and photoelectrochemical performance of Ag@m-TiO_2 nanocomposite. Sol. Energy Mater. Sol. Cells 141, 162–170.
Aribisala, J.O., Sabiu, S., 2022. Redox impact on bacterial macromolecule: a promising avenue for discovery and development of novel antibacterials. Biomolecules 12 (11), 1545.
Athanassiou, C.G., Kavallieratos, N.G., Benelli, G., Losic, D., Usha Rani, P., Desneux, N., 2018. Nanoparticles for pest control: current status and future perspectives. J. Pest. Sci. 91 (1), 1–15.
Aygün, A., Özdemir, S., Gülcan, M., Cellat, K., Sen, F., 2020. Synthesis and characterization of Reishi mushroom-mediated green synthesis of silver nanoparticles for the biochemical applications. J. Pharm. Biomed. Anal. 178, 112970.
Aygün, A., Özdemir, S., Gülcan, M., Yalçın, M.S., Uçar, M., Şen, F., 2022. Characterization and antioxidant-antimicrobial activity of silver nanoparticles synthesized using Punica granatum extract. Internat J. Environ Sci Tech. 19 (4), 2781–2788.
Balamurugan, V., Muruganandam, L., Natarajan, R., 2022. Photocatalytic activity of silver nanoparticles synthesized using *Cadiospermum halicacabum* and *Moringa oleifera* leaf extract. Mater. Today Proc. 62 (8), 5365-5370.
Balouiri, M., Sadiki, M., Ibnsouda, S.K., 2016. Methods for in vitro evaluating antimicrobial activity: a review. J. Pharmaceut Analy. 6 (2), 71–79.
Barua, S., Raul, P.K., Gopalakrishnan, R., Das, B., Veer, V., 2016. Sustainable-resource-based carbon dot–silver nanohybrid: a strong tool against *Culex quinquefasciatus*, a common disease vector. ACS Sustain. Chem. Eng. 4 (4), 2345–2350.
Bharadwaj, K.K., Rabha, B., Pati, S., Choudhury, B.K., Sarkar, T., Gogoi, S.K., Kakati, N., Baishya, D., Kari, Z.A., Edinur, H.A., 2021. Green synthesis of silver nanoparticles using *Diospyros malabarica* fruit extract and assessments of their antimicrobial, anticancer and catalytic reduction of4-nitrophenol (4-NP). Nanomaterials 11, 1999.
Bibi, I., Maqbool, H., Iqbal, S., Majid, F., Kamal, S., Alwadai, N., Iqbal, M., 2021. La1-xGdxCr1-yNiyO3 perovskite nanoparticles synthesis by micro-emulsion route: dielectric, magnetic and photocatalytic properties evaluation. Ceram. Int. 47 (4), 5822–5831.
Bostanci, M.T., Bulbul, A.S., Celik, I.S., Kocabas, Y.Z., Burhan, H., Bayat, R., Karimi-Maleh, H., 2022. Investigation of antibacterial, antifungal, antibiofilm, antioxidant and anticancer properties of methanol extracts of *Salvia marashica* Ilçim, Celep & Doğan and Salvia caespitosa Montbret & Aucher ex Benth plants with medicinal importance. Chemosphere 288, 132602.
Chandhru, M., Logesh, R., Kutti Rani, S., Ahmed, N., Vasimalai, N., 2022. Green synthesis of silver nanoparticles from plant latex and their antibacterial and photocatalytic studies. Environ. Technol. 43 (20), 3064–3074.
Chinnappan, S., Kandasamy, S., Arumugam, S., Seralathan, K.K., Thangaswamy, S., Muthusamy, G., 2018. Biomimetic synthesis of silver nanoparticles using flower extract of *Bauhinia purpurea* and its antibacterial activity against clinical pathogens. Environ. Sci. Pollut. Res. 25 (1), 963–969.
Clinical and Laboratory Standards Institute, 2015. CLSI document M07-A10. In: Methods for Dilution of Antimicrobial Susceptibility Tests for Bacteria that Grow Aerobically; Approved Standard—10th Edition. Clinical and Laboratory Standards Institute (Wayne, PA).
Dheyab, M.A., Aziz, A.A., Jameel, M.S., Noqta, O.A., Mehrdel, B., 2020. Synthesis and coating methods of biocompatible ironoxide/gold nanoparticle and nanocomposite for biomedical applications. Chin. J. Phys. 64, 305–325.
Diana, E.J., Mathew, T.V., 2022. Synthesis and Characterization of Surface-Modified Ultrafine Titanium Dioxide Nanoparticles with an Antioxidant Functionalized Biopolymer as a Therapeutic Agent: Anticancer and Antimicrobial Evaluation. Colloids and Surfaces B: Biointerfaces, 112949.
Dridi, R., Essghaier, B., Hannachi, H., Khedher, G.B., Chaffei, C., Zid, M.F., 2022. Biosynthesized silver nanoparticles using *Anagallis monelli*: evaluation of antioxidant activity, antibacterial and antifungal effects. J. Mol. Struct. 1251, 132076.
Elumalai, D., Hemavathi, M., Deepaa, C.V., Kaleena, P.K., 2017. Evaluation of phytosynthesised silver nanoparticles from leaf extracts of *Leucas aspera* and *Hyptis suaveolens* and their larvicidal activity against malaria, dengue and filariasis vectors. Parasite Epidem Contr 2 (4), 15–26.
Erenler, R., Dag, B., 2022. Biosynthesis of silver nanoparticles using *Origanum majorana* L. and evaluation of their antioxidant activity. Inorganic and Nano-Metal Chem. 52 (4), 485–492.
Finney, D.J., 1971. Probit Analysis. Cambridge University Press, London, pp. 68–72.
Foster, W.A., Walker, E.D., 2019. Mosquitoes (Culicidae). In: Medical and Veterinary Entomology. Academic press, pp. 261–325.
Frieri, M., Kumar, K., Boutin, A., 2017. Antibiotic resistance. J. Inf. Publ. Health 10 (4), 369–378.
Ga'al, H., Fouad, H., Mao, G., Tian, J., Jianchu, M., 2018. Larvicidal and pupicidal evaluation of silver nanoparticles synthesized using *Aquilaria sinensis* and *Pogostemon cablin* essential oils against dengue and zika viruses vector Aedes albopictus mosquito and its histopathological analysis. Artificial cells. Nanomed. Biotechnol. 46 (6), 1171–1179.
Gebre, S.H., 2022. Bio-inspired synthesis of metal and metal oxide nanoparticles: the key role of phytochemicals. J. Cluster Sci. 1–40.
Gol, F., Aygün, A., Seyrankaya, A., Gür, T., Yenikaya, C., Sen, F., 2020. Green synthesis and characterization of Camellia sinensis mediated silver nanoparticles for antibacterial ceramic applications. Mater. Chem. Phys. 250, 1–11, 123037.
Gulbagca, F., Ozdemir, S., Gulcan, M., Sen, F., 2019. Synthesis and characterization of *Rosa canina*-mediated biogenic silver nanoparticles for anti-oxidant, antibacterial, antifungal, and DNA cleavage activities. Heliyon 5, e02980, 1-6.
Gupta, R., Pandit, C., Pandit, S., Gupta, P.K., Lahiri, D., Agarwal, D., Pandey, S., 2022. Potential and future prospects of biochar-based materials and their applications in removal of organic contaminants from industrial wastewater. J. Mater. Cycles Waste Manag. 1–25.
Hemlata, P.R.M., Pratap Singh, A., Tejavath, K.K., 2020. Biosynthesis of silver nanoparticles using Cucumis prophetarum aqueous leaf extract and their antibacterial and antiproliferative activity against cancer cell lines. ACS Omega 10, 5520–5528.
Jadoun, S., Arif, R., Jangid, N.K., Meena, R.K., 2021. Green synthesis of nanoparticles using plant extracts: a review. Environ. Chem. Lett. 19 (1), 355–374.
Jahan, I., Erci, F., Isildak, I., 2021. Rapid green synthesis of non-cytotoxic silver nanoparticles using aqueous extracts of' Golden Delicious' apple pulp and cumin seeds with antibacterial and antioxidant activity. SN Appl. Sci. 3 (1), 1–14.
Jeevanandam, J., Kiew, S.F., Boakye-Ansah, S., Lau, S.Y., Barhoum, A., Danquah, M.K., Rodrigues, J., 2022. Green approaches for the synthesis of metal and metal oxide nanoparticles using microbial and plant extracts. Nanoscale 14 (7), 2534–2571.
Jeong, G.J., Khan, S., Tabassum, N., Khan, F., Kim, Y.M., 2022. Marine-bioinspired nanoparticles as potential drugs for multiple biological roles. Mar. Drugs 20 (8), 527.
Karimi, F., Ayati, A., Tanhaei, B., Sanati, A.L., Afshar, S., Kardan, A., Dabirifar, Z., Karaman, C., 2022a. Removal of metal ions using a new magnetic chitosan nano-bio-adsorbent; A powerful approach in water treatment. Environ. Res. https://doi.org/10.1016/j.envres.2021.111753.
Karimi, F., Rezaei-Savadkouhi, N., Uçar, M., Aygun, A., Tiri, R.N.E., Meydan, I., Sen, F., 2022. Efficient green photocatalyst of silver-based palladium nanoparticles for methyle orange photodegradation, investigation of lipid peroxidation inhibition, antimicrobial, and antioxidant activity. Food Chem. Toxicol. 169, 113406.
Kaur, M., Gautam, A., Guleria, P., Singh, K., Kumar, V., 2022. Green Synthesis of Metal Nanoparticles and Their Environmental Applications. Current Opinion in Environmental Science & Health, 100390.
Khursheed, A., Rather, M.A., Jain, V., Rasool, S., Nazir, R., Malik, N.A., Majid, S.A., 2022. Plant based natural products as potential ecofriendly and safer biopesticides: a comprehensive overview of their advantages over conventional pesticides, limitations and regulatory aspects. Microb. Pathog., 105854
Kumar, P., Govindaraju, M., Senthamilselvi, S., Premkumar, K., 2013. Photocatalytic degradation of methyl orange dye using silver (Ag) nanoparticles synthesized from *Ulva lactuca*. Colloids Surf., B 103, 658–661.
Labulo, A.H., David, O.A., Terna, A.D., 2022. Green synthesis and characterization of silver nanoparticles using *Morinda lucida* leaf extract and evaluation of its antioxidant and antimicrobial activity. Chem. Pap. 1–13.
Li, Q., Yu, S., Han, J., Wu, J., You, L., Shi, X., Wang, S., 2022. Synergistic antibacterial activity and mechanism of action of nisin/carvacrol combination against *Staphylococcus aureus* and their application in the infecting pasteurized milk. Food Chem. 380, 132009.
Liang, K.H., Som, S., Gupta, K.K., Lu, C.H., 2022. Electrochemical characterization of TiNb2O7 as anode material synthesized using microwave assisted micro emulsion route. J. Am. Ceram. Soc. 105 (12), 7446-7454.
Liang, Y., Demir, H., Wu, Y., Aygun, A., Tiri, R.N.E., Gur, T., Vasseghian, Y., 2022. Facile synthesis of biogenic palladium nanoparticles using biomass strategy and application as photocatalyst degradation for textile dye pollutants and their *in-vitro* antimicrobial activity. Chemosphere 306, 135518.
Liao, S., Zhang, Y., Pan, X., Zhu, F., Jiang, C., Liu, Q., Chen, L., 2019. Antibacterial activity and mechanism of silver nanoparticles against multidrug-resistant Pseudomonas aeruginosa. Int. J. Nanomed. 14, 1469.
Lin, J., Gulbagca, F., Aygun, A., Tiri, R.N.E., Xia, C., Van Le, Q., Vasseghian, Y., 2022. Phyto-mediated synthesis of nanoparticles and their applications on hydrogen generation on NaBH4, biological activities and photodegradation on azo dyes: development of machine learning model. Food Chem. Toxicol. 163, 112972.
Mallikarjuna, K., Nasif, O., Ali Alharbi, S., Chinni, S.V., Reddy, L.V., Reddy, M.R.V., Sreeramanan, S., 2021. Phytogenic synthesis of Pd-Ag/rGO nanostructures using stevia leaf extract for photocatalytic H2 production and antibacterial studies. Biomolecules 11 (2), 190.
Mares-Briones, F., Barragán-Mares, O., López-Miranda, J., Esparza, R., Rosas, G., 2019. Bimetallic Ag@ Pt core-shell nanoparticles and their catalytic activity by a green approach. Mater. Res. Express 6, 0850h0858.
Loi, M., Paciolla, C., Logrieco, A.F., Mulè, G., 2020. Plant bioactive compounds in pre- and postharvest management for aflatoxins reduction. Front. Microbiol. 11, 243.

Madhu, C.S., Balaji, K.S., Shankar, J., Gowda, S.S., Sharada, A.C., 2022. Biofabrication of silver nanoparticles using *Praecitrullus fistulosus* fruit extract exhibits *in vitro* antibacterial and anticancer activity. J. Drug Deliv. Sci. Technol. 72, 103329.
Malafaia, G., de Souza, A.M., Pereira, A.C., Gonçalves, S., da Costa Araújo, A.P., Ribeiro, R.X., Rocha, T.L., 2020. Developmental toxicity in zebrafish exposed to polyethylene microplastics under static and semi-static aquatic systems. Sci. Total Environ. 700, 134867.
Maleki, P., Nemati, F., Gholoobi, A., Hashemzadeh, A., Sabouri, Z., Darroudi, M., 2021. Green facile synthesis of silver-doped cerium oxide nanoparticles and investigation of their cytotoxicity and antibacterial activity. Inorg. Chem. Commun. 131, 108762.
Marimuthu, S., Antonisamy, A.J., Malayandi, S., Rajendran, K., Tsai, P.C., Pugazhendhi, A., Ponnusamy, V.K., 2020. Silver nanoparticles in dye effluent treatment: a review on synthesis, treatment methods, mechanisms, photocatalytic degradation, toxic effects and mitigation of toxicity. J. Photochem. Photobiol. B Biol. 205, 111823.
Mechouche, M.S., Merouane, F., Messaad, C.E.H., Golzadeh, N., Vasseghian, Y., Berkani, M., 2022. Biosynthesis, characterization, and evaluation of antibacterial and photocatalytic methylene blue dye degradation activities of silver nanoparticles from *Streptomyces tuirus* strain. Environ. Res. 204, 112360.
Miri, A., Sarani, M., Bazaz, M.R., Darroudi, M., 2015. Plant-mediated biosynthesis of silver nanoparticles using *Prosopis farcta* extract and its antibacterial properties. Spectrochim. Acta part a: Molecul and Biomol Spect. 141, 287–291.
Mondal, A., Sen, K., Mondal, A., Mishra, D., Debnath, P., Mondal, N.K., 2022. Bio-fabricated silver nanoparticles for controlling dengue and filaria vectors and their characterization, as well as toxicological risk assessment in aquatic mesocosms. Environ. Res. 212, 113309.
Mughal, S.S., Hassan, S.M., 2022. Comparative study of AgO nanoparticles synthesize via biological, chemical and physical methods: a review. American J. Materials Synthesis Process 7 (2), 15–28.
Murugan, N., Srinivasan, R., Murugan, A., Kim, M., Natarajan, D., 2020. *Glycosmis pentaphylla* (Rutaceae): a Natural candidate for the isolation of potential bioactive Arborine and Skimmianine compounds for controlling multidrug-resistant *Staphylococcus aureus*. Front. Public Health 8, 176. https://doi.org/10.3389/fpubh.2020.00176.
Musiime, A.K., Krezanoski, P.J., Smith, D.L., Kilama, M., Conrad, M.D., Otto, G., Tusting, L.S., 2022. House design and risk of malaria, acute respiratory infection and gastrointestinal illness in Uganda: a cohort study. PLOS Global Publ. Health 2 (3), e0000063.
Mustapha, T., Misni, N., Ithnin, N.R., Daskum, A.M., Unyah, N.Z., 2022. A review on plants and microorganisms mediated synthesis of silver nanoparticles, role of plants metabolites and applications. Int. J. Environ. Res. Publ. Health 19 (2), 674.
Nagalingam, M., Kalpana, V.N., Panneerselvam, A., 2018. Biosynthesis, characterization, and evaluation of bioactivities of leaf extract-mediated biocompatible gold nanoparticles from *Alternanthera bettzickiana*. Biotech. Rep. 19, e00268.
Nasir, S., Walters, K.F., Pereira, R.M., Waris, M., Chatha, A.A., Hayat, M., Batool, M., 2022. Larvicidal activity of acetone extract and green synthesized silver nanoparticles from *Allium sativum* L.(Amaryllidaceae) against the dengue vector *Aedes aegypti* L.(Diptera: Culicidae). J. Asia Pac. Entomol., 101937
Nawabjohn, M.S., Sivaprakasam, P., Anandasadagopan, S.K., Begum, A.A., Pandurangan, A.K., 2021. Green synthesis and characterisation of silver nanoparticles using *Cassia tora* seed extract and investigation of antibacterial potential. Appl. Biochem. Biotechnol. 1–15.
Negi, A., Rana, P., Negi, D.S., 2022. Multi dye degradation, antibacterial, antidiabetic and antioxidant assessment of silver nanoparticles (Ag-NPs) derived via leaves of Smilax aspera. Inorg. Chem. Commun., 109703
Nikam, A.V., Prasad, B.L.V., Kulkarni, A.A., 2018. Wet chemical synthesis of metal oxide nanoparticles: a review. CrystEngComm 20 (35), 5091–5107.
Nirmala, C., Sridevi, M., 2021. Characterization, antimicrobial and antioxidant evaluation of biofabricated silver nanoparticles from Endophytic *Pantoea anthophila*. J. Inorg. Organomet. Polym. Mater. 31 (9), 3711–3725.
Ntoumba, A.A., Meva, F.E.A., Ekoko, W.E., Foko, L.P.K., Hondt, E.N., Schlüsener, C., Lehman, L.G., 2019. Biogenic synthesis of silver nanoparticles using Guava (*Psidium guajava*) leaf extract and its larvicidal action against *Anopheles gambiae*. J. Biomaterials Nanobiotechnol. 11 (1), 49.
OECD, 2012. Chemicals Testing Guidelines. http://www.oecd.org/department/0,3355,en_2649_34377_1_1_1_1_1,00.html. (Accessed 12 February 2012). Accessed.
Ojha, S., 2022. Green synthesis of metallic nanoparticles: advancements and future perspectives. Biol. Sci. 2 (3), 262–268.
Oliver, S., Wagh, H., Liang, Y., Yang, S., Boyer, C., 2018. Enhancing the antimicrobial and antibiofilm effectiveness of silver nanoparticles prepared by green synthesis. J. Math. Chem. B 6 (24), 4124–4138.
Parthiban, E., Manivannan, N., Ramanibai, R., Mathivanan, N., 2019. Green synthesis of silver-nanoparticles from Annona reticulata leaves aqueous extract and its mosquito larvicidal and anti-microbial activity on human pathogens. Biotech Rep. 21, e00297.
Patel, M., 2022. Green synthesis of nanoparticles: a solution to environmental pollution. In: Handbook of Solid Waste Management. Springer, Singapore, pp. 1965–1993.
Periyasami, G., Palaniappan, S., Karuppiah, P., Rahaman, M., Karthikeyan, P., Aldalbahi, A., Al-Dhabi, N.A., 2022. Biogenic silver nanoparticles fabricated by *Euphorbia granulata* Forssk's extract: investigating the antimicrobial, radical scavenging, and catalytic activities. J. Nanomater. 2022.
Qiang, L., Arabeyyat, Z.H., Xin, Q., Paunov, V.N., Dale, I.J., Lloyd Mills, R.I., Cheng, J., 2020. Silver nanoparticles in Zebrafish (*Danio rerio*) embryos: uptake, growth and molecular responses. Int. J. Mol. Sci. 21 (5), 1876.
Rajasekar, R., Thanasamy, R., Samuel, M., Edison, T.N.J.I., Raman, N., 2022. Eco-friendly synthesis of silver nanoparticles using *Heterotheca subaxillaris* flower and its catalytic performance on reduction of methyl orange. Biochem. Eng. J., 108447
Rajkumar, G., Sundar, R., 2022. Biogenic one-step synthesis of silver nanoparticles (AgNPs) using an aqueous extract of Persea americana seed: Characterization, phytochemical screening, antibacterial, antifungal and antioxidant activities. Inorg. Chem. Commun. 143, 109817.
Rajput, S., Kumar, D., Agrawal, V., 2020. Green synthesis of silver nanoparticles using Indian Belladonna extract and their potential antioxidant, anti-inflammatory, anticancer and larvicidal activities. Plant Cell Rep. 39 (7), 921–939.
Ravichandran, V., Vasanthi, S., Shalini, S., Shah, S.A.A., Tripathy, M., Paliwal, N., 2019. Green synthesis, characterization, antibacterial, antioxidant and photocatalytic activity of Parkia speciosa leaves extract mediated silver nanoparticles. Results Phys. 15, 102565.
Renuka, R., Renuka Devi, K., Sivakami, M., Thilagavathi, T., 2021. *Solanum torvum* mediated synthesis and characterization of silver nanoparticles for antibacterial activities. J. Plant Biochem. Biotechnol. 30 (3), 596–601.
Rizwana, H., Alwhibi, M.S., Al-Judaie, R.A., Aldehaish, H.A., Alsaggabi, N.S., 2022. Sunlight-mediated green synthesis of silver nanoparticles using the berries of *Ribes rubrum* (red currants): characterisation and evaluation of their antifungal and antibacterial activities. Molecules 27 (7), 2186.
Sahin Yaglioglu, A., Erenler, R., Gecer, E.N., Genc, N., 2022. Biosynthesis of silver nanoparticles using *Astragalus flavesces* Leaf: identification, antioxidant activity, and catalytic degradation of methylene blue. J. Inorg. Organomet. Polym. Mater. 1–8.
Salem, A., Saion, E., Al-Hada, N.M., Kamari, H.M., Shaari, A.H., Abdullah, C.A.C., Radiman, S., 2017. Synthesis and characterization of CdSe nanoparticles via thermal treatment technique. Results Phys. 7, 1556–1562.
Sap-Iam, N., Homklinchan, C., Larpudomlert, R., Warisnoicharoen, W., Sereemaspun, A., Dubas, S.T., 2010. UV irradiation-induced silver nanoparticles as mosquito larvicides. J. Appl. Sci. 10 (23), 3132–3136.
Satsangi, N., Preet, S., 2021. Phyto-synthesis and Characterization of Potent Larvicidal Silver Nanoparticles Using Nyctanthes arbortristis Leaf Extract. J. Plant Biochem. Biotechnol. 30 (3), 608–612.
Seckin, H., Tiri, R.N.E., Meydan, I., Aygun, A., Gunduz, M.K., Sen, F., 2022. An environmental approach for the photodegradation of toxic pollutants from wastewater using Pt–Pd nanoparticles: antioxidant, antibacterial and lipid peroxidation inhibition applications. Environ. Res. 208, 112708.
Şengül Demirak, M.Ş., Canpolat, E., 2022. Plant-based bioinsecticides for mosquito control: impact on insecticide resistance and disease transmission. Insects 13 (2), 162.
Srikar, S.K., Giri, D.D., Pal, D.B., Mishra, P.K., Upadhyay, S.N., 2016. Green synthesis of silver nanoparticles: a review. Green Sustain. Chem. 6 (1), 34–56.
Subramaniam, S., Kumarasamy, S., Narayanan, M., Ranganathan, M., Rathinavel, T., Chinnathambi, A., Whangchai, K., 2022. Spectral and structure characterization of Ferula assafoetida fabricated silver nanoparticles and evaluation of its cytotoxic, and photocatalytic competence. Environ. Res. 204, 111987.
Taran, M., Rad, M., Alavi, M., 2016. Characterization of Ag nanoparticles biosynthesized by Bacillus sp. HAI4 in different conditions and their antibacterial effects. J. Appl. Pharmaceut. Sci. 6 (11), 94–99.
Thamer, A., Murad, A., 2020. Facile one pot microwave-assisted green synthesis of Fe2 O 3/Ag nanocomposites by phytoreduction: potential application as sunlight-driven photocatalyst, antibacterial and anticancer agent. J. Photochem. Photobiol. B Biol. 207, 111885-111885.
Tiri, R.N.E., Gulbagca, F., Aygun, A., Cherif, A., Sen, F., 2022. Biosynthesis of Ag–Pt bimetallic nanoparticles using propolis extract: antibacterial effects and catalytic activity on NaBH4 hydrolysis. Environ. Res. 206, 112622.
Valgas, C., Souza, S.M.D., Smânia, E.F., Smânia Jr., A., 2007. Screening methods to determine antibacterial activity of natural products. Braz. J. Microbiol. 38, 369–380.
Venkatesh, N., Aravindan, S., Ramki, K., Murugadoss, G., Thangamuthu, R., Sakthivel, P., 2021. Sunlight-driven enhanced photocatalytic activity of bandgap narrowing Sn-doped ZnO nanoparticles. Environ. Sci. Pollut. Res. 28 (13), 16792–16803.
WHO, 2005. Guidelines for Laboratory and Field Testing of Mosquito Larvicides. WHO, Geneva, Switzerland.
Wilson, J.J., Lakshmi, M.P., Sivakumar, T., Ponmanickam, P., Sevarkodiyone, S.P., 2022. Green synthesis of silver nanoparticles using Bacillus subtilis (P3) and its larvicidal, histopathological and biotoxicity efficacy. South Afr. J.
Wilson-Bahun, T.A., Kamgang, B., Lenga, A., Wondji, C.S., 2020. Larval ecology and infestation indices of two major arbovirus vectors, Aedes aegypti and Aedes albopictus (Diptera: Culicidae), in Brazzaville, the capital city of the Republic of the Congo. Parasites & Vectors 13 (1), 1–18.
Xiao, F., Xu, T., Lu, B., Liu, R., 2020. Guidelines for antioxidant assays for food components. Food Front 1 (1), 60–69.
Yang, M., Lu, F., Zhou, T., Zhao, J., Ding, C., Fakhri, A., Gupta, V.K., 2020. Biosynthesis of nano bimetallic Ag/Pt alloy from Crocus sativus L. extract: biological efficacy and catalytic activity. J. Photochem. Photobiol. B Biol. https://doi.org/10.1016/j.jphotobiol.2020.112025.
Yin, I.X., Zhang, J., Zhao, I.S., Mei, M.L., Li, Q., Chu, C.H., 2020. The antibacterial mechanism of silver nanoparticles and its application in dentistry. Int. J. Nanomed. 15, 2555.
Yousaf, S., Zulfiqar, S., Shahi, M.N., Warsi, M.F., Al-Khalli, N.F., Aboud, M.F.A., Shakir, I., 2020. Tuning the structural, optical and electrical properties of NiO nanoparticles prepared by wet chemical route. Ceram. Int. 46 (3), 3750–3758.
Zhang, L., Wei, Y., Wang, H., Wu, F., Zhao, Y., Liu, X., Su, H., 2020. Green synthesis of silver nanoparticles using mushroom Flammulina velutipes extract and their antibacterial activity against aquatic pathogens. Food Bioprocess Technol. 13 (11), 1908–1917.
Zhao, D., Wang, S., Hu, Y., Liu, X., Tao, J., Sagratini, G., Xiang, Q., 2022. Insight into the antibacterial activity of lauric arginate against Escherichia coli O157: H7: membrane disruption and oxidative stress. LWT 162, 113449.